npj | parkinson's disease

Article

Published in partnership with the Parkinson's Foundation

https://doi.org/10.1038/s41531-024-00853-5

Multiomics approach identifies dysregulated lipidomic and proteomic networks in Parkinson's disease patients mutated in *TMEM175*

Federica Carrillo[1], Marco Ghirimoldi[2], Giorgio Fortunato[1], Nicole Piera Palomba[3], Laura Ianiro[3], Veronica De Giorgis[2], Shahzaib Khoso[2,4], Tiziana Giloni[3], Sara Pietracupa[3,5], Nicola Modugno[3], Elettra Barberis[4,6], Marcello Manfredi[2,7,8] & Teresa Esposito[1,3,8]

Parkinson's disease (PD) represents one of the most frequent neurodegenerative disorders for which clinically useful biomarkers remain to be identified and validated. Here, we adopted an untargeted omics approach to disclose lipidomic, metabolomic and proteomic alterations in plasma and in dermal fibroblasts of PD patients carrying mutations in *TMEM175* gene. We revealed a wide dysregulation of lysosome, autophagy, and mitochondrial pathways in these patients, supporting a role of this channel in regulating these cellular processes. The most significant altered lipid classes were Fatty acyls, Glycerophospholipids and Phosphosphingolipids. The plasma level of Phosphatidylcholines (PC) and Phosphatidylinositol (PI) 34:1 significantly correlated with an earlier age at onset of the disease in TMEM175 patients ($p = 0.008$; $p = 0.006$). In plasma we also observed altered amino acids metabolic pathways in PD patients. We highlighted that increased level of L-glutamate strongly correlated ($p < 0.001$) with the severity of motor and non-motor symptoms in PD_TMEM175 patients. In dermal fibroblasts, we disclosed alterations of proteins involved in lipids biosynthesis (PAG15, PP4P1, GALC, FYV1, PIGO, PGPS1, PLPP1), in the insulin pathway (IGF2R), in mitochondrial metabolism (ACD10, ACD11, ACADS) and autophagy (RAB7L). Interestingly, we quantified 43 lysosomal or lysosomal-related proteins, which were differentially modulated between TMEM175 patients and controls. Integrative correlation analysis of proteome and lipidome of PD_TMEM175 cellular models identified a strong positive correlation of 13 proteins involved in biosynthetic processes with PC and Ceramides. Altogether, these data provide novel insights into the molecular and metabolic alterations underlying *TMEM175* mutations and may be relevant for PD prediction, diagnosis and treatment.

Parkinson's disease (PD) pathophysiology is still an aim of study in the neurodegeneration field due to the complex aetiology[1]. The effective pathological characteristic of PD is the progressive loss of dopaminergic (DA) neurons in the Substantia Nigra pars compacta (SNpc) and the accumulation of intracellular α-synuclein in the form of Lewy-body[2]. Diagnosis of PD relies on clinical history, physical examination, and the response to dopaminergic drugs, but misdiagnosis is common in the early phases of the disease. PD is now considered to be a diverse group of disorders, rather than a single pathogenic disease entity, affecting both the peripheral and central nervous system[3,4]. For this reason, new approaches

[1]Institute of Genetics and Biophysics "Adriano Buzzati-Traverso", National Research Council, Naples, Italy. [2]Biological Mass Spectrometry Lab, Department of Translational Medicine, University of Piemonte Orientale, Novara, Italy. [3]IRCCS INM Neuromed, Pozzilli, Italy. [4]Center for Translational Research on Autoimmune and Allergic Diseases, University of Piemonte Orientale, Novara, Italy. [5]Department of Human Neuroscience, Sapienza University of Rome, Piazzale Aldo Moro, Italy. [6]Department of Sciences and Technological Innovation, University of Piemonte Orientale, Alessandria, Italy. [7]IRCCS Policlinico San Donato, Institute of Molecular and Translational Cardiology, Milan, Italy. [8]These authors contributed equally: Marcello Manfredi, Teresa Esposito. e-mail: teresa.esposito@igb.cnr.it

for the study of PD should be adopted by combining multiple omics layers of high-throughput sources to elucidate new biological information for a better understanding of neurodegenerative conditions. Particularly, metabolomic, proteomic and lipidomic analyses are spreading as new tools to widely investigate pathway alterations in PD patients within biological fluids, cellular models and tissues, which could better reflect PD process. Lipids, metabolites, and proteins reflect the physiological and pathological status of an individual. Profiling these data types could be useful not only to highlight new pathways affected in PD condition but also to identify sensitive and effective markers for early disease detection and potentially effective therapeutic interventions. In fact, it has been suggested that precision medicine applied to PD should be based on biomarker profiles instead of clinical features, which can change rapidly within a few years and largely overlap[4]. Although much progress has been made in the last years in PD biomarkers research, clinically useful biochemical markers remain to be identified and validated for early and more precise diagnosis of PD or for differentiation of subtypes of PD, which may require different treatments. Biomarkers are also needed to predict the course of the disease, including possible adverse effects of dopamine replacement strategies, the development of levodopa-induced dyskinesia (LID), and to monitor the effect of experimental disease-modifying treatments in the future.

However, the majority of reported studies have been conducted in PD cohorts not stratified at the genetic level or focusing the attention on PD patients carrying mutations in the most common genes associated with the disease, such as *LRRK2*, *SNCA*, *PRKN* and *PINK*[5–9], which not recapitulate all the complex genetic background of PD patients.

Our previous studies and recent evidence indicated *TMEM175* as an emerging new risk gene for Parkinson's disease[10–13]. Haoxing Xu's group demonstrated how TMEM175 functioning is crucial to ensure lysosomal pH stability and consequently lysosomal functioning[14]. The knocking out of TMEM175 was demonstrated to induce loss of dopaminergic neurons and impairment in motor function in mice[15]. Recently, we functionally characterised several likely pathogenic variants in *TMEM175* gene occurring in about 5% of the Italian PD cohort and we described how these variants affected channel activity, autophagy, and unfolded protein response (UPR) signalling pathways[11].

Thus, based on this evidence, in this study we investigated whether the presence of mutation in *TMEM175* gene could reflect a characteristic lipidomic, metabolomic and proteomic signature of PD patients both at circulating and cellular level. The study cohort included two groups of PD patients and a group of healthy subjects matched for age and sex. PD patients were matched for clinical parameters, but they differ for the presence of mutation in *TMEM175* gene. PD patients carrying no mutation in *TMEM175* were carriers of variants in other PD genes not directly related to the lysosome pathway. The aim of the study was to identify new altered metabolic pathways and potential biomarkers at circulating level associated with the presence of mutation in *TMEM175* gene in PD patients.

Results

This work utilises genomic, lipidomic, metabolomic, and proteomic approaches to investigate the molecular constituents of pathways that may be disrupted in PD patients with mutation in *TMEM175* gene (Fig. 1). The analysis focuses on plasma circulating biofluid and dermal fibroblasts. The PD cohort includes 804 unrelated PD patients who were recruited before and during the pandemic period from 2015 to 2017 and from 2021 to 2022. All patients were investigated with the same study protocol that included the evaluation of motor and non-motor symptoms (see "Methods"). We conducted whole exome sequencing (WES) analysis of the entire cohort, and we identified 30 different variants in *TMEM175* gene in 63 patients (about 8% of the entire cohort), suggesting an important role of this gene in PD risk (Table S1 reports the complete list of variants identified in our study cohort) (Carrillo et al., 2024, under revision). For this study, we selected 25 out of the 63 PD patients (referred to as PD_TMEM175) who were recruited before the pandemic period (from 2015 to 2017) and for which demographic and clinical information were available (Table 1). This choice was made to avoid stratification of the study cohort due to the different length of time of conservation of the biological samples and to metabolic alterations that could be due to SARS-CoV-2 infection. Overall, the selected group of patients was carrier of 16 different likely pathogenic variants that affected the functionality of TMEM175 channel, as recently demonstrated (Table S2)[11]. We also selected a group of PD patients referred to as PD_NoTMEM175 carrying both no mutations in PD genes ($N = 8$) and rare variants in PD genes not involved in the lysosomal pathway ($N = 6$) (Table S2). A group of healthy subjects ($N = 14$ and referred to as Controls) matched for sex and age was included in the study (Table 1). No significant differences were identified with respect to sex, age, body mass index (BMI), and serum cholesterol concentration from High- and Low-Density Lipoproteins between PD and healthy subjects (Table 1). The two groups of PD patients were matched for motor and non-motor symptoms (Table 1).

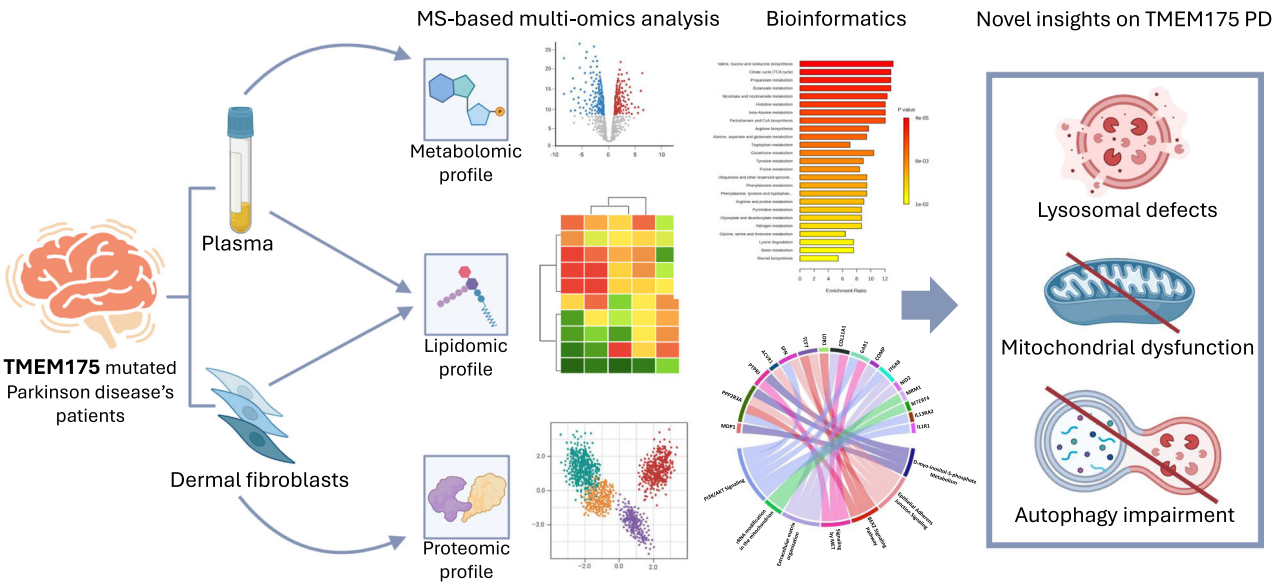

Fig. 1 | Workflow. Graphical representation of the study. The figure was created with BioRender.com (www.biorender.com).

Table 1 | Demographic and clinical characteristics of the study cohort

Clinical features	Controls *N* = 14	PD_TMEM175 *N* = 25	PD_NoTMEM175 *N* = 14	CTR vs PD_TMEM175 *p*-value	CTR vs PD_NoTMEM175 *p*-value	PD_TMEM175 vs PD_NoTMEM175 *p*-value
Sex % (males)	78%	64%	57%			
Age	70.4 ± 4.3	66.1 ± 10.2	71.5 ± 5	0.1436	0.5380	0.0720
BMI	27 ± 2.71	26.8 ± 2.9	25.6 ± 4.9	0.8349	0.3581	0.3473
Cholesterol mg/dl	172.2 ± 35.8	148.8 ± 41.9	163.2 ± 37.6	0.0890	0.5223	0.2963
HDL mg/dl	115.2 ± 57.7	102.3 ± 46.4	98.3 ± 57.5	0.4549	0.4446	0.8158
LDL/VLDL mg/dl	74.1 ± 35.1	56.2 ± 46.4	67.4 ± 36.4	0.2203	0.6242	0.4443
AAO	–	58.3 ± 9.4	64 ± 6.9			0.0558
Disease duration	–	7.92 ± 5	7.2 ± 3.4			0.6348
H&Y	–	2.04 ± 0.9	1.9 ± 1			0.6568
UPDRS III	–	21.6 ± 11.7	28 ± 20.1			0.2148
NMS	–	58.2 ± 41.7	79.2 ± 75.2			0.2735
MoCA	–	23.3 ± 4.5	25.6 ± 5.4			0.1626
LID	–	12/25	3/14			0.0954

The values were represented as mean ± standard deviation. The two-tailed *T*-test was used to calculate *p*-value of cohort variables Age, BMI, AAO, Disease duration, H&Y, UPDRS III, NMS and MoCA in two groups of patients; *p*-value of LID was calculated with Fisher's exact test.
BMI body mass index, *HDL* high-density lipoproteins, *LDL/VLDL* low-density lipoproteins/very low-density lipoproteins, *AAO* age at onset, *H&Y* Hoehn and Yahr, *UPDRS* Unified Disease Rating Scale, *NMS* Non-Motor Symptoms score, *MoCA* Montreal Cognitive Assessment, *LID* levodopa-induced dyskinesia.

Analysis of plasma samples: PD patients carrying TMEM175 mutation revealed a specific alteration of plasma lipidomic profile

To explore whether the presence of mutation in *TMEM175* gene in PD patients could have an impact on lipid metabolism, we performed liquid chromatography coupled with high-resolution mass spectrometry analysis of plasma samples identifying 901 expressed lipid species belonging to 24 lipid classes (Fig. S1a, b). Hierarchical clustering analysis as well as unsupervised and supervised analyses through Principal Component Analysis (PCA) and Partial Least Squares Discriminant Analysis (PLS-DA), discriminated between the two groups at circulating level in PD patients (both PD_TMEM175 and PD_NoTMEM175 patients) when compared to healthy subjects (Figs. 2a–d and S1c–f).

Expression analysis identified 15 downregulated (Fold Change (FC) ≤ 0.65; $p \leq 0.01$) and 364 upregulated (FC ≥ 1.5; $p \leq 0.01$) lipid species when comparing PD_TMEM175 versus healthy subjects (Fig. 3a, Table S3). 18 downregulated and 31 upregulated lipid species were identified by the contrast PD_NoTMEM175 versus healthy subjects (Fig. 3b). The complete lists of lipids identified in the two contrasts are reported in Tables S4 and S5. These data showed that the majority of lipid classes were increased specifically in PD patients carrying *TMEM175* mutations (Fig. 3c–f). Hierarchical heatmap as well as *t*-test analysis showed that the most significantly increased lipid classes in these patients belonged to Fatty Acyls (Acylcarnitines (CAR), Fatty acid (FA), N-acyl ethanolamine (NAE)), Glycerophospholipids (Phosphatidylcholine (PC), Lysophosphatidylcholine (LPC), Ether-linked Phosphatidylethanolamine (PE O-), Phosphatidylinositol (PI), Ether-linked Phosphatidylcholine (PC O-)) and Sphingolipids (Ceramide (Cer), Hexosylceramide (HexCer) and Sphingomyelin (SM)) (Figs. 4a–c, S2, Table S6). Only the Cholesteryl Esters (CEs) were significantly downregulated in both groups of PD patients (Figs. 4a–c and S2). In addition, these results open to further investigation of lipoprotein levels since the directional change of many lipid classes might be the consequence of changes in lipoprotein abundance.

Analysis of plasma samples: metabolomic profile in plasma samples highlighted altered amino acids metabolism in TMEM175 PD patients

Metabolomic analysis of circulating molecules was conducted in plasma samples of the same study cohort in which we performed lipidomic analysis to explore the presence of altered metabolic pathways, which could be uniquely observed in PD patients with *TMEM175* mutation. Hierarchical heatmap and PCA analyses reflected metabolic changes in PD patients (PD_TMEM175 and PD_NoTMEM175) compared to control subjects (Fig. 5a–d). Interestingly, both PD groups of patients were well clustered based on the abundance of molecules, suggesting the presence of a different metabolic profile in the two groups of patients. In PD_TMEM175 patients we detected 460 metabolites including 35 significantly increased (FC ≥ 1.5; $p \leq 0.01$) and 15 significantly decreased molecules (FC ≤ 0.65; $p \leq 0.01$) with respect to controls (Fig. 6a). In PD_NoTMEM175 group we detected 455 metabolites including 31 significantly increased (FC ≥ 1.5; $p \leq 0.01$) and 55 significantly decreased molecules (FC ≤ 0.65; $p \leq 0.01$) (Fig. 6b). Looking at the specific metabolite levels we observed significantly increased levels of L-Threonine, L-Tyrosine, L-Aspartate, L-Glutamine, L-Asparagine, L-Lysine, L-Glutamate, L-Tryptophan in PD_NoTMEM175 patients, while in TMEM175 patients we only found significant decreased level of L-Aspartate (Table S7). Enrichment pathway analysis, performed in the KEGG database, displayed pathways specifically altered in PD patients (PD_TMEM175 and PD_NoTMEM175), which were involved in the amino acid metabolism. The most significantly impacted pathways identified in both groups were tryptophan, histidine and beta-alanine metabolism, as well as lysine degradation, suggesting an altered energy metabolism in PD patients (Fig. 6c–f, Tables S8 and S9).

Analysis of plasma samples: correlation analysis of lipids and metabolites with PD endophenotypes

Linear regression analysis was performed by comparing demographic (age and sex) and clinical features (age at onset (AAO), motor symptoms (UPDRS score), non-motor symptoms (NMS total score), mood and cognition (D3 domain), gastrointestinal-trait alteration (D6 domain), cognitive impairment (MoCA score), Levodopa Equivalent Dose (LEED), years of L-dopa treatment and years of disease duration) with the concentrations of the lipids and metabolites among the most significantly deregulated in PD TMEM175 patients. Overall data showed that the levels of several lipids were negatively or positively correlated with age and age at onset of the disease as well as the concentration of several amino acids correlated with the severity of motor and non-motor symptoms (Figs. S3 and S4, Tables S10–S12). The most significant contrasts observed with linear regression analysis were analysed with

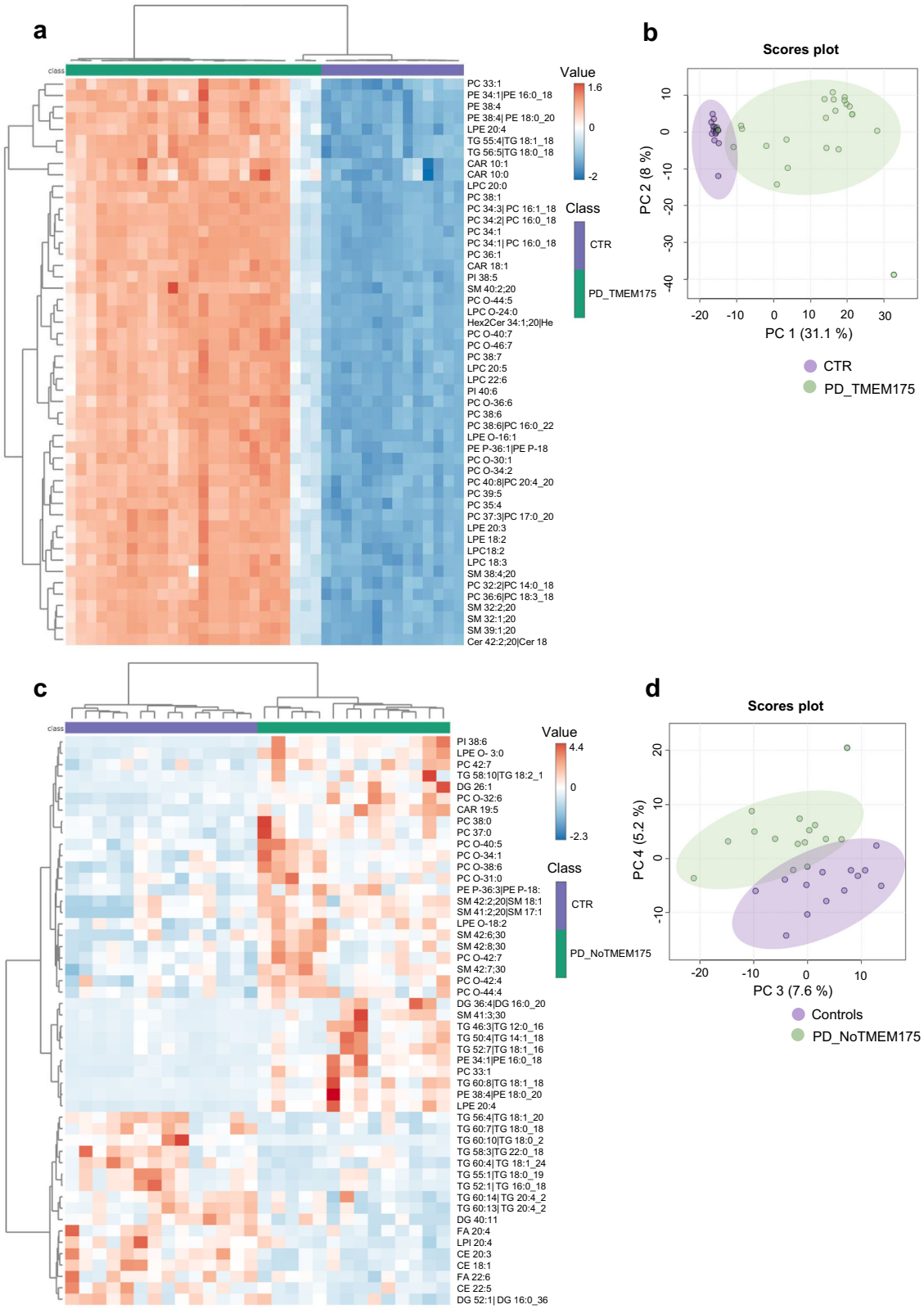

Fig. 2 | Heatmap representation and unsupervised PCA of plasma lipids. **a**, **b** Heatmap representation of the most 50 differentially expressed lipid species highlighting the clusters of the two groups of analysis when comparing PD_TMEM175 (**a**) and PD_NoTMEM175 (**b**) versus the Control subjects. **c**, **d** Unsupervised PCA displayed a well separation of the groups of analysis reflecting the percentage of contribution of PC1 and PC2 to the variance by comparing PD_TMEM175 (**c**) and PD_NoTMEM175 (**d**) to the control group.

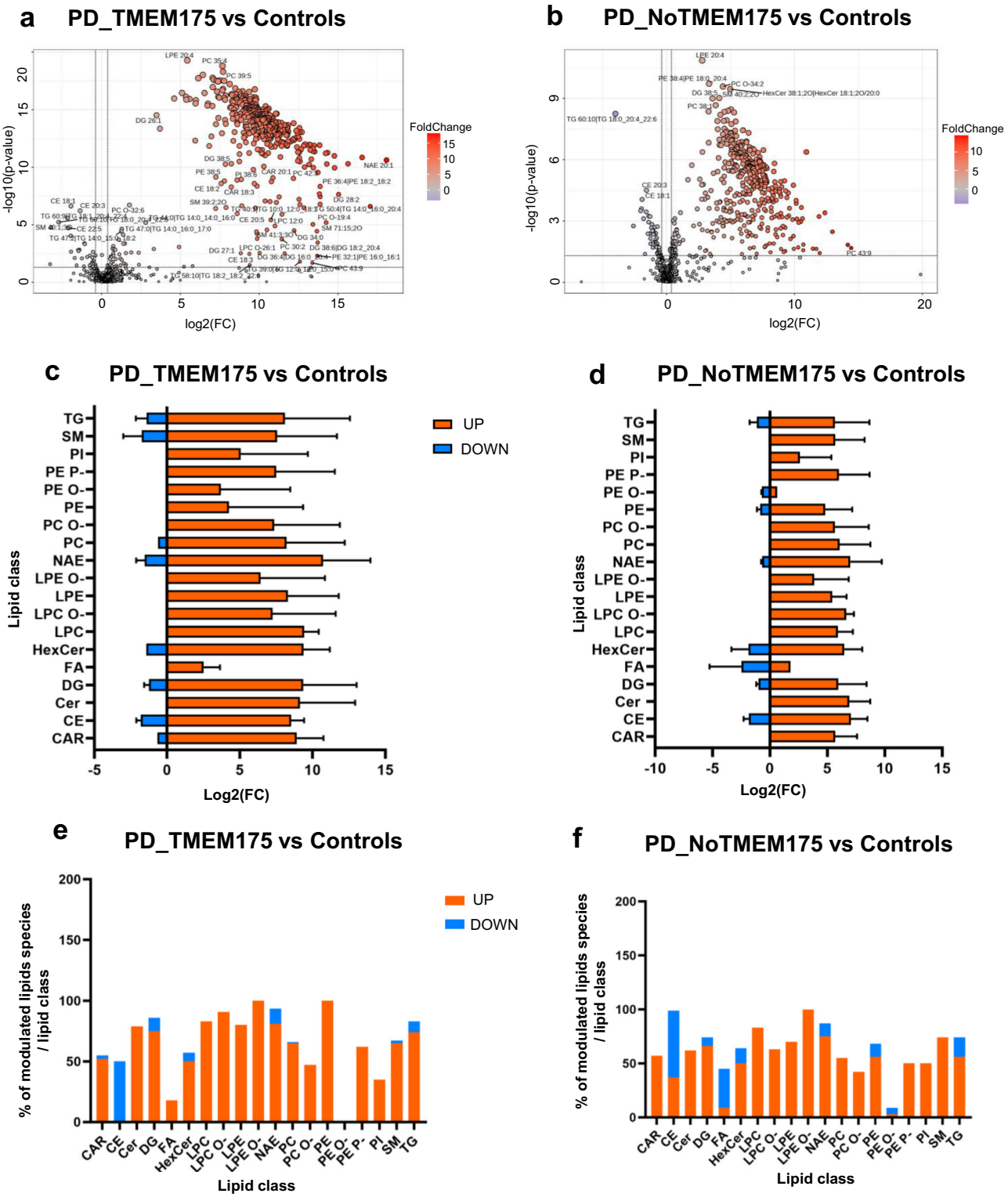

Fig. 3 | Altered lipid distribution in plasma samples of PD_TMEM175 group. **a**, **b** Volcano plot showed the distribution of the most significant altered lipid species comparing PD_TMEM175 vs Control (**a**) and PD_NoTMEM175 vs Control group (**b**). Lipids showing statistically significant different expression are in the top right (upregulated) and top left (downregulated) quadrants. The black line represents the *p*-value threshold set to $p < 0.01$. Lipid species significantly altered reflecting a wide upregulation of lipids in the group of PD_TMEM175 with respect to the PD-NoTMEM175 compared to the control ones. **c**, **d** Comparison of the circulating lipid expression of the PD_TMEM175 patients versus the control samples (**c**) and of the PD_NoTMEM175 patients versus the control samples (**d**). Data are shown as mean ± Standard Deviation (SD) of Log2 Fold Change (FC). Lipid species were considered with $0.65 \leq FC \geq 1.5$. **e**, **f** The two contrasts PD_TMEM175 (**e**) and PD_NoTMEM175 (**f**) versus controls reflected an increased percentage of lipid species in the most of lipid class except for Cholesterol Esters (CE) in both groups of PD patients.

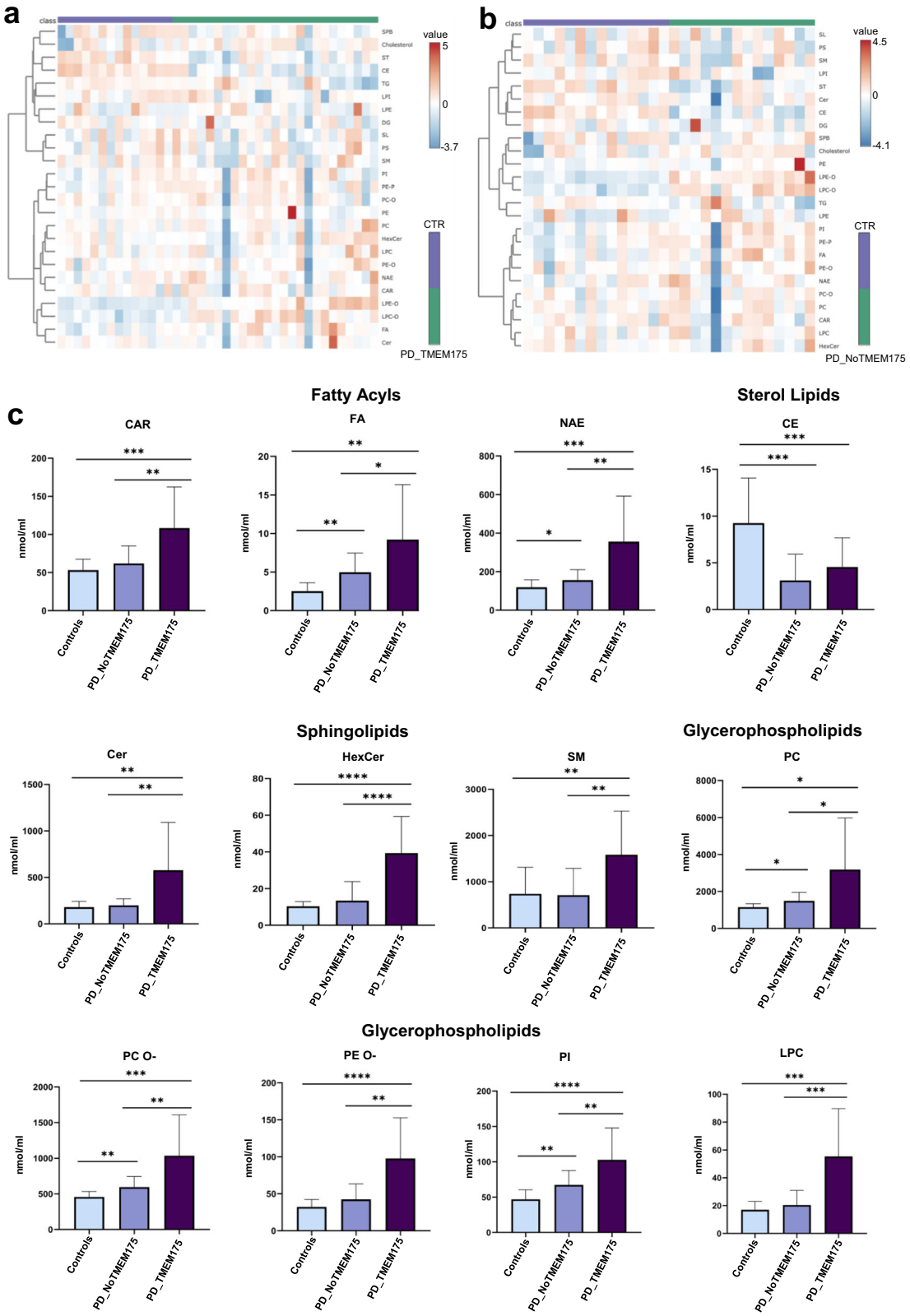

Fig. 4 | The plasma concentration of the most altered lipid classes in PD_TMEM175 group. a, **b** Hierarchical heatmap showed clustering of lipid classes in both PD_TMEM175 (**a**) and PD_NoTMEM175 (**b**) with respect to the control group. **c** Comparison of plasma concentration of the most dysregulated lipid classes in PD_TMEM175 patients displayed a significant increase of Fatty Acyls (CAR, FA and NAE), Sphingolipids (Cer, HexCer and SM), Glycerophospholipids (PC, PC O-, PE O-, PI and LPC) with respect to both the control subjects and PD_NoTMEM175 patients. Data are represented as mean ± SD and were analysed with unpaired *T*-test. ****p-value < 0.0001, ***p-value < 0.001, **p-value < 0.01, *p-value < 0.05.

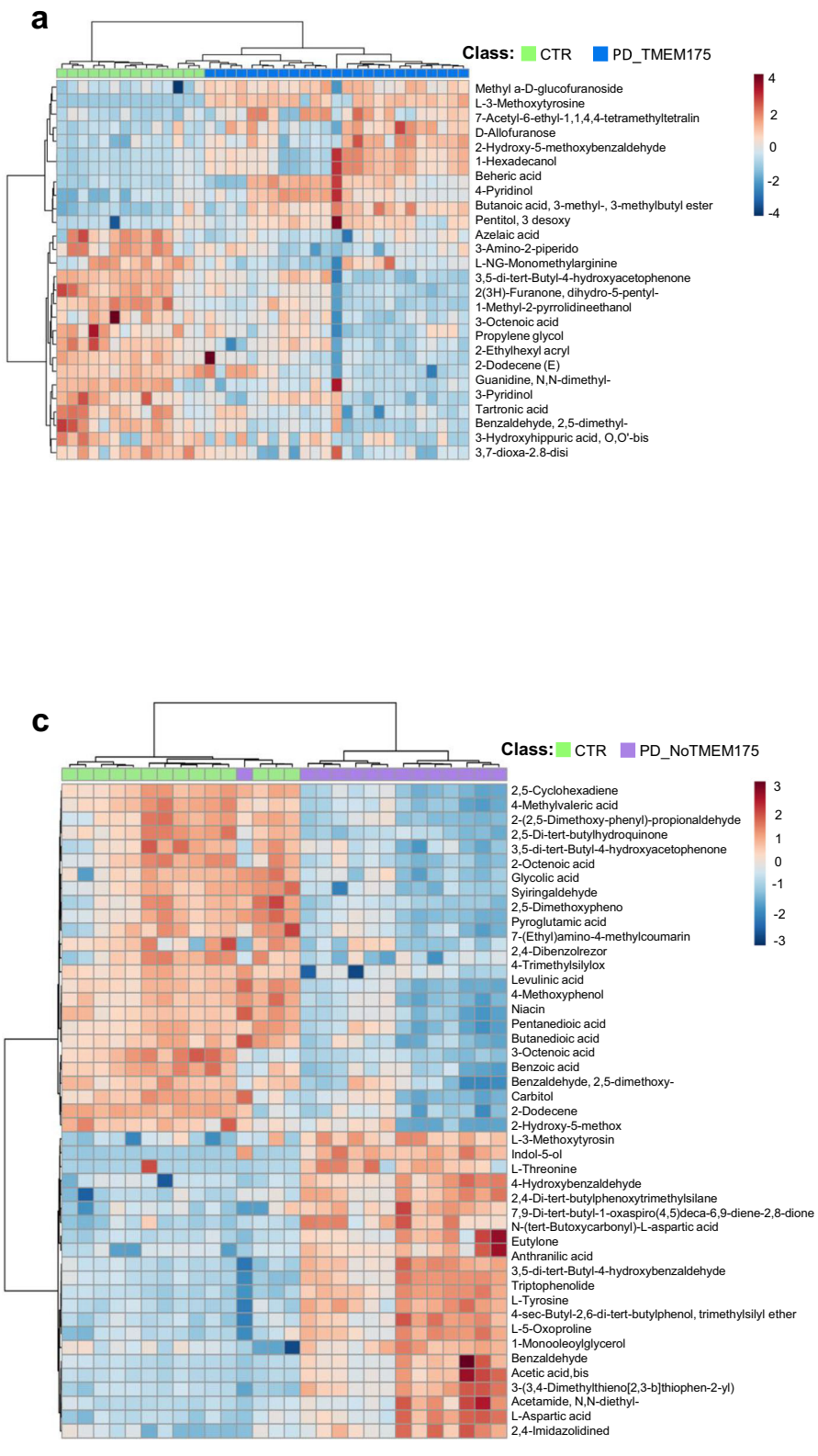

Fig. 5 | Analysis of metabolomic profile in plasma samples. a, **c** Heatmap representation of the most significant representative metabolites displayed discrimination between the PD_TMEM175 (**a**) and PD_NoTMEM175 (**c**) groups with respect to the control one. **b**, **d** Principal component analysis (PCA) showed two defined groups of analysis indicating differences in metabolome profile by considering PD_TMEM175 (**b**) and PD_NoTMEM175 (**d**) compared to the controls.

Pearson correlation and corrected for multiple tests. The results are reported in Fig. 7a–c. PC and PI34:1/PI:16:0_18:1 negatively correlated with age and AAO in PD_TMEM175 patients (PC vs age $r = -0.56$, $p = 0.0054$; PC vs AAO $r = -0.53$, $p = 0.0083$; PI34:1 vs age $r = -0.55$, $p = 0.0061$; PI34:1 vs AAO $r = -0.55$, $p = 0.0064$) (Fig. 7a, b). In PD_TMEM175 the plasma concentration of L-Glutamic acid positively correlated with the severity of motor (UPDRS score; $r = 0.64$, $p = 0.0008$) and non-motor symptoms (NMS score; $r = 0.67$, $p = 0.0005$), as well as with the severity of gastrointestinal defects (D6 score; $r = 0.72$, $p = 0.0001$) (Fig. 7c).

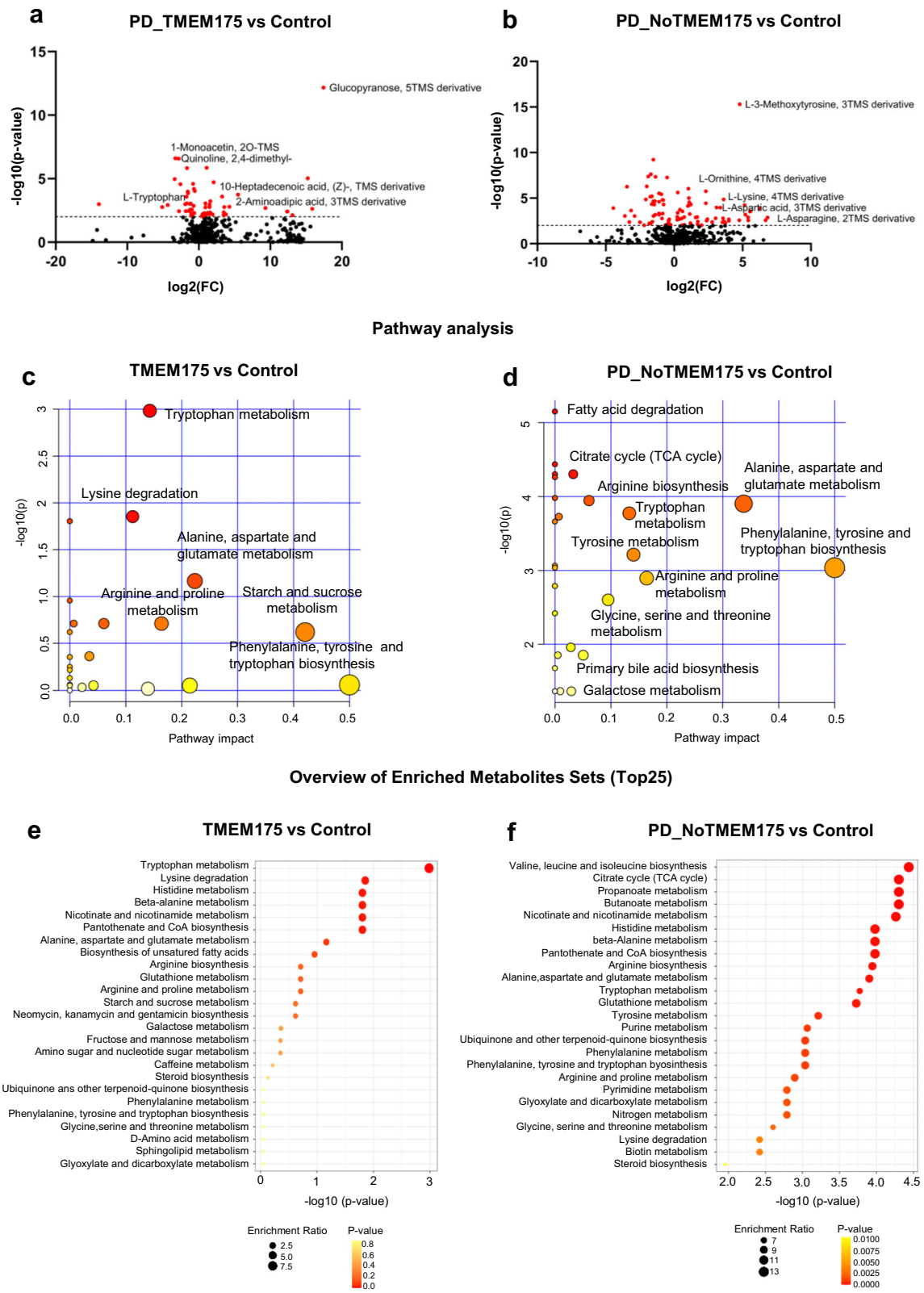

Fig. 6 | Dysregulation of amino acid pathways in plasma of PD patients. **a**, **b** Volcano plot showed the most significant altered metabolites by comparing both PD_TMEM175 (**a**) and PD_NoTMEM175 (**b**) vs the Control group. Red dots represented metabolites significantly altered reflecting a minor number of modulated molecules in the group of PD_TMEM175. The black line represents the *p*-value threshold set to $p \leq 0.01$. **c**–**f** Metabolome view of pathway impact analysis obtained from metabolites differentially expressed in PD_TMEM175 (**c**, **e**) and PD_NoTMEM175 (**d**, **f**) compared to the controls. Data showed an enrichment of pathways involved in amino acid metabolism in PD_TMEM175 group. The colour and size of each circle are based on *p*-values (yellow: higher *p*-values and red: lower *p*-values) and pathway impact values (the larger the circle the higher the impact score) calculated from the topological analysis, respectively. Pathways were considered significantly enriched if $p \leq 0.05$, impact 0.1 and number of metabolite hits in the pathway >1.

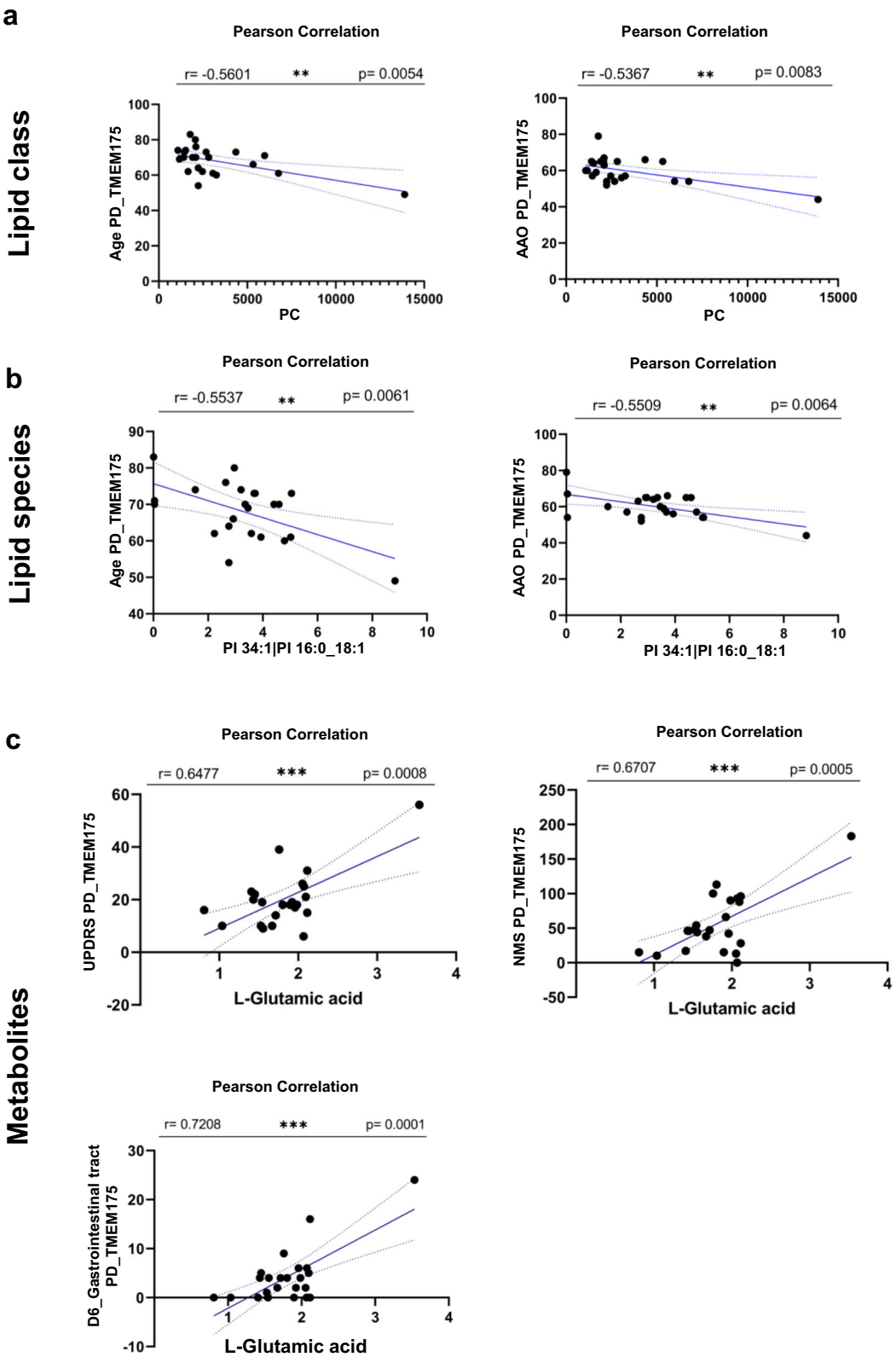

Fig. 7 | Levels of lipids and metabolites in plasma of TMEM175 patients correlated with PD endophenotypes. a, **b** Graphical representation of the significant negative correlation of the levels of PC and PI 34:1|PI 16:0_18:1 with age and age at onset (AAO) in PD_TMEM175 patients. **c** L-Glutamic acid showed a significant positive correlation with UPDRS, NMS and D6 Gastrointestinal trait score in PD_TMEM175 patients. Correlation was evaluated with Pearson analysis and *p*-value was corrected with Bonferroni multiple testing. *r* and *p*-value (*p*) were reported in the graph for each analysis.

Analysis of patient-derived dermal fibroblasts: lipidomic profile of PD_TMEM175 cellular models confirmed a marked dysregulation of specific lipid classes

To explore the lipidomic signature in PD cells, we cultured human dermal fibroblasts derived from both PD patients carrying *TMEM175* gene mutation ($N = 6$), PD patients carrying no mutation in *TMEM175* gene ($N = 4$) and controls ($N = 2$). Although only two control cell lines were used, and thus caution should be made on reading the following results, both the cell lines derived from neurologically and cognitively healthy ageing subjects recruited before pandemic period and were analysed by WES to exclude the presence of variants in PD genes. The number of fibroblast cell lines of patients and controls recruited for this study was comparable to other studies reported in literature[7,16,17]. Considering the crucial role of TMEM175 in autophagy and UPR signalling pathways, as recently described[11], we collected cellular samples after 1 h of nutrient deprivation to potentially boost the autophagy pathway. Experiments were performed on cells with equal passage numbers, ranging from 5 to 10, to avoid artefacts due to senescence, known to occur at passage numbers greater than 30. Analyses were carried out in four independent biological replicates.

A wide dysregulation of lipid species was observed in the cells of both groups of PD patients (PD_TMEM175 and PD_NoTMEM175) (Figs. 8a–d, S5a–d).

We identified 1184 expressed lipid species belonging to 28 lipid classes. We found 35 significant upregulated ($FC \geq 1.5$; $p \leq 0.01$) and 203 significant downregulated lipids ($FC \leq 0.65$; $p \leq 0.01$) in patients carrying *TMEM175* mutation compared to controls (Fig. 9a). 170 significant upregulated and 329 downregulated lipid species were identified by the contrast PD_NoTMEM175 versus healthy subjects (Fig. 9b). The complete lists of lipids identified in the two contrasts are reported in Tables S13 and S14. In the dermal fibroblasts of PD_TMEM175 patients, we observed increased levels of CAR, HexCer, and several lipid classes belonging to Glycerophospholipids (PE, PE-O, PG, and PI). In these cell lines, we also observed decreased levels of Cer, PC, PC-O, differently from what was observed in plasma (Figs. 9c–e, S6, Table S15). Among the presented data we observed a strong increase of PC in healthy subjects that could be taken with caution. We can not exclude that this data could be due to the variability among controls' replicates and to the presence of only two control cell lines (Fig. 9e). Additional analyses are required to confirm this data.

Interestingly, focusing on lysosomal or lysosomal-related lipids we observed in the dermal fibroblasts of PD patients increased levels of Bis(Monoacylglycero)Phosphate (BMP), and HexCer, as well as decreased levels of SM, Cer, and Sphingoid bases (SPB) (Fig. 9e). The increase in BMP might suggest the expansion of the endo-lysosomal compartment as observed in storage disorders[18], which could be in accordance with the nuclear translocation of the transcription factor TFEB, that we recently described in the same PD cells[11].

Sixty-two lipid species, shared between cells and plasma, were significantly altered in the contrast PD_TMEM175 versus controls; the most altered lipid species were reported in Table S16. The majority of lipids belonging to PC, Cer and TG were decreased in fibroblast cell lines and increased in plasma. Instead, a significant increase of CAR 16:0, CAR 16:1, CAR 16:2, CAR 18:2, CAR 18:3, CAR 20:4, LPC 18:0, SM 41:3;3O, PE 36:3 and PI 36:3 was observed in fibroblasts and in plasma in *TMEM175* patients (Table S16).

Analysis of patient-derived dermal fibroblasts: proteomic profile of dermal fibroblasts derived from PD patients carrying *TMEM175* mutation highlighted alteration of lysosomal and mitochondrial proteins

To perform a comprehensive analysis of the presence of altered metabolic pathways in PD patients we investigated the proteomic profile in the same set of dermal fibroblasts in which we conducted the lipidomic analysis. Proteomic analysis identified 6676 proteins that were quantified across all the samples. Statistical analysis showed the presence of hundreds of modulated proteins when comparing data from PD_TMEM175 patients versus healthy subjects (Fig. 10a). Protein enrichment analysis in terms of cellular components, performed with DAVID database, identified a high dysregulation in lysosome, mitochondria and extracellular matrix' proteins supporting the hypothesis that mutations occurring in TMEM175 could affect lysosome and mitochondria functioning (Fig. 10b). We discovered a decreased level of several key enzymes working at lysosome, autophagosome, endoplasmic reticulum (ER), and plasma membrane, including PAG15, PP4P1, GALC, FYV1, PIGO, PGPS1 and PLPP1 in PD_TMEM175. All these enzymes, but GALC which is responsible for Sphingomyelin production, are involved in Glycerophospholipids biosynthesis[19]. Strikingly, the group of PD_TMEM175 patients also exhibited downregulation of several proteins related to insulin and glucose metabolism pathways, including AHSG, ALB, C3, ITIH2, SERPINC1, IF2B1, MPRI, GLUT-6 and GLUT-10 (Table S17). We also observed a highly significant reduced level of proteins involved in autophagic-lysosomal pathways such as CATK, CATF and CATL1, which are involved in protein degradation[20] and RAB7L, an autophagy-related protein, recently associated with PD[21]. Interestingly, among the identified proteins, we were able to quantify more than 200 lysosomal or lysosomal-related proteins, of which, 43 were differentially modulated between PD_TMEM175 and controls (Tables 2, S18). In addition, network analysis of these regulated proteins, highlighted a strong interaction of lysosomal and lysosomal membrane proteins, supporting the impact of TMEM175 mutations in lysosomal pathways (Fig. 10c, d). However, among the modulated lysosomal proteins, except cathepsin K (CTSK) and N-sulfoglucosamine sulfohydrolase (SGSH), which were significantly decreased especially in TMEM175 patients, we observed the same trend in the two groups of PD patients, supporting that lysosome dysfunction is common in Parkinson's disease, regardless of the type of gene mutation[22].

Moreover, we discovered a significant downregulation of enzymes implicated in numerous finely regulated mitochondrial processes, like mitochondrial translation, ATP biosynthesis, mitochondrial organisation, and response to oxidative stress. Among these enzymes, we identified the Acyl-CoA dehydrogenase family members 10 and 11 (ACD10 and ACD11) and the Short-chain specific acyl-CoA dehydrogenase (ACADS), involved in fatty acid beta-oxidation and degradation (Table S17). Ingenuity Pathway Analysis (IPA) identified several important metabolic pathways affected in PD patients mutated in *TMEM175* gene (Fig. 11a). Of relevance for this study was the identification of two important deregulated pathways such as PI3K/AKT signalling and D-myoinositol synthesis and metabolism. In particular, AKT acts as a direct modulator of TMEM175[15], while Myo-inositol is crucial for producing phosphoinositide, which interacts with α-synuclein, and is involved in the intracellular signalling[23–26]. The proteins involved in some top pathways such as PI3K/AKT (PPP2R3A, SFN, GAB1, ITGA8, IL13RA2 and IL1R1), D-myoinositol-5-phosphate (MDP1, PPP2R3A and PTPRJ), and extracellular matrix organization (COL11A1, COMP, ITGA8 and NID2) are reported in Fig. 11b and in Table S19.

Analysis of patient-derived dermal fibroblasts: integrative correlation analysis of proteome and lipidome of PD_TMEM175 cellular models

The correlations between proteomics and lipidomics data were evaluated using a supervised multi-omics integrative analysis which maximises the correlations between different types of omics and identify key molecules which can discriminate different sample groups[27]. This integration was used to investigate the relationship between proteins and lipids across TMEM175 and No_TMEM175 cell models.

The integrated model selected proteins and lipids that best explain TMEM175 mutation-related variations. The general correlations between proteome and lipidome were high (0.79 for TMEM175 and 0.88 for No_TMEM175, respectively), suggesting common information among multi-omics results (Fig. 12a, d). A circus plot of the identified correlations between the two groups of PD patients is presented in Fig. 12b, e. A strong positive correlation between proteins and lipids was found in both

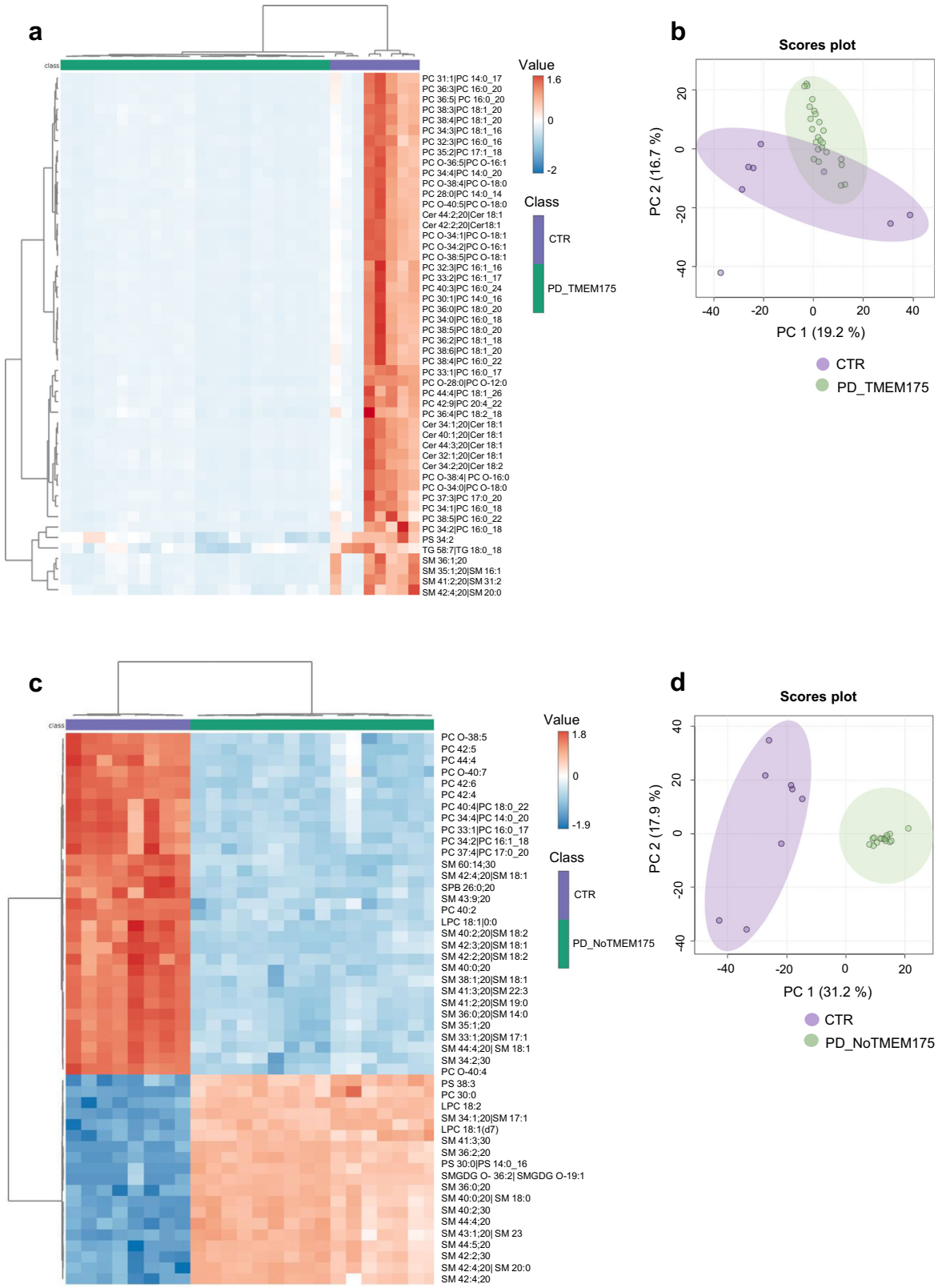

Fig. 8 | Heatmap representation and unsupervised PCA of cellular lipids. **a**, **c** Heatmap representation showed the presence of two groups of analysis and confirmed a wide dysregulation of lipid species at cellular level when comparing both PD_TMEM175 (**a**) and PD_NoTMEM175 groups (**c**) with respect to control one. **b**, **d** PCA showed a well separation of the two groups of PD patients compared to the controls.

experimental models. Negative correlations were less abundant compared to the positive ones but more present in PD_NoTMEM175 samples. The correlation within the same sample group may indicate functional or physical lipid–protein interaction.

To explore the differences in the protein–lipid association among PD patients, we conducted a topological analysis of protein–lipid correlation networks (Fig. 12c, f). Networks were built using all strongly correlating lipid–protein pairs selected in each sample group based on significant strong

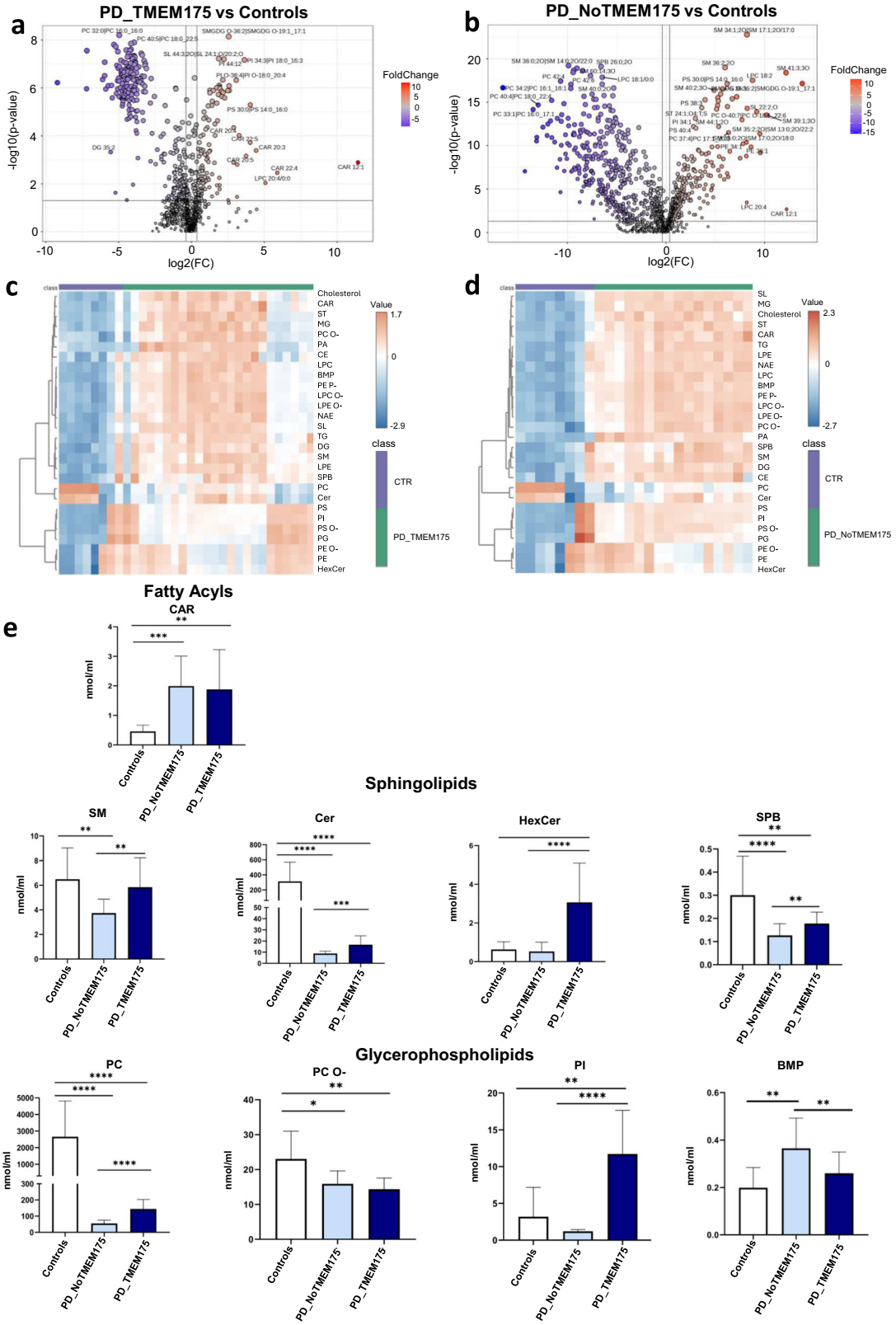

Fig. 9 | Altered lipid distribution in human dermal fibroblasts. a, **b** Volcano plot representation of altered expressed lipid species showed a wide downregulation of lipid species at cellular level in the group of PD_TMEM175. Lipid species were selected with p-value ≤ 0.01 and FC ≤0.65 and ≥1.5. **c**, **d** Hierarchical heatmap displayed clustering of lipid classes among PD_TMEM175 (**c**) and PD_NoTMEM175 (**d**) compared to the control group. **e** The most dysregulated lipid classes in PD_TMEM175 patients were CAR, HexCer and PI. Data are represented as mean ± SD and were analysed with unpaired T-test. ****p-value < 0.0001, ***p-value < 0.001, **p-value < 0.01, *p-value < 0.05.

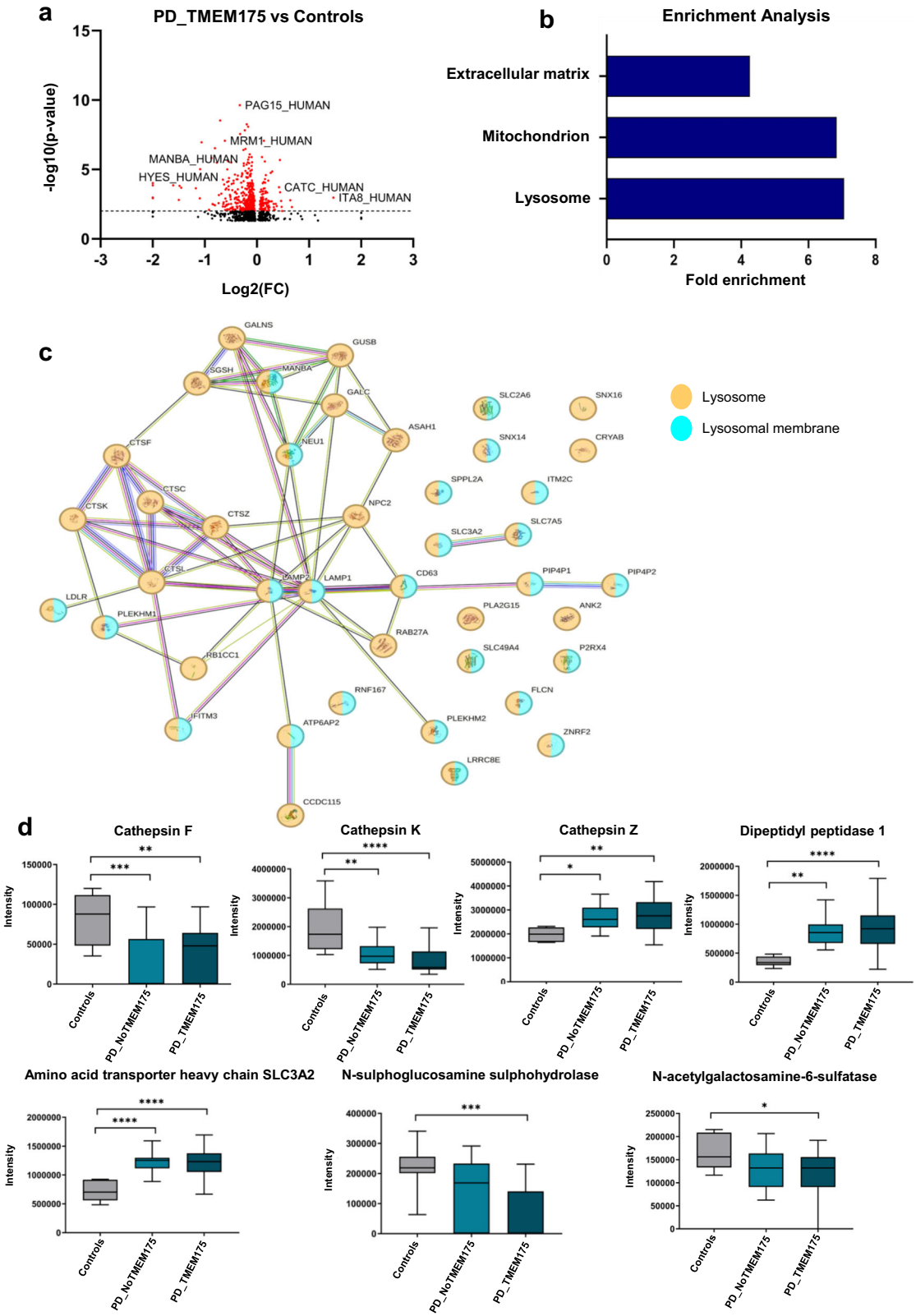

Fig. 10 | PD_TMEM175 patients displayed alteration of lysosomal and mitochondrial proteins. a Volcano plot showed the most significantly altered proteins comparing PD_TMEM175 vs Controls. Red dots represented proteins significantly altered reflecting a higher number of downregulated proteins in PD_TMEM175 compared to the controls. The black line represents the *p*-value threshold set to $p \leq 0.01$. **b** Proteomic profile of PD_TMEM175 group compared to controls was evaluated by pathway enrichment analysis in terms of cellular components. The analysis, performed in the DAVID database, showed an enrichment of proteins localised into the extracellular matrix, lysosome and mitochondrion. Data were represented as fold enrichment value. **c** Protein-protein interaction analysis of the modulated lysosomal and lysosomal-related proteins in PD_TMEM175 patients was performed in STRING database. The result showed an interaction node of about 26 proteins found to be modulated in PD_TMEM175 patients. **d** Boxplots showed the abundance of the most modulated lysosomal and lysosomal-related proteins in the three groups of analysis. *p*-value was evaluated by ONE-way ANOVA, $^{*}p < 0.05$, $^{**}p < 0.01$, $^{***}p < 0.001$ and $^{****}p < 0.0001$.

Table 2 | Altered lysosomal and lysosomal-related proteins in dermal fibroblasts derived from patients carrying *TMEM175* mutation

ID	Name	Gene	Fold change	*p*-value
O00462	Beta-mannosidase	MANBA	0.13	1.53E-06
P54803	Galactocerebrosidase	GALC	0.15	3.83E-03
P51688	N-sulfoglucosamine sulfohydrolase	SGSH	0.28	7.20E-05
Q9Y5W7	Sorting nexin-14	SNX14	0.37	4.40E-04
Q6NSJ5	Volume-regulated anion channel subunit LRRC8E	LRRC8E	0.40	1.70E-02
P43235	Cathepsin K	CTSK	0.40	5.13E-05
Q8NFG4	Folliculin	FLCN	0.46	2.24E-02
P13473	Lysosome-associated membrane glycoprotein 2 (LAMP-2)	LAMP2	0.46	2.00E-02
Q8NCC3	Phospholipase A2 group XV (1-O-acylceramide synthase)	PLA2G15	0.46	2.33E-10
Q8NHG8	E3 ubiquitin-protein ligase ZNRF2	ZNRF2	0.47	3.47E-02
Q9UBX1	Cathepsin F	CTSF	0.49	2.24E-03
Q9Y4G2	Pleckstrin homology domain-containing family M member 1	PLEKHM1	0.5	3.46E-02
Q9H6Y7	E3 ubiquitin-protein ligase RNF167	RNF167	0.51	3.53E-02
Q8TCT8	Signal peptide peptidase-like 2A	SPPL2A	0.52	3.03E-02
Q96NT0	Coiled-coil domain-containing protein 115	CCDC115	0.53	7.80E-04
Q86T03	Type 1 phosphatidylinositol 4.5-bisphosphate 4-phosphatase	PIP4P1	0.58	2.91E-02
Q9UGQ3	Solute carrier family 2. facilitated glucose transporter member 6 (Glucose transporter type 6) (GLUT-6)	SLC2A6	0.59	2.54E-03
P57768	Sorting nexin-16	SNX16	0.61	4.62E-03
Q99519	P2X purinoceptor 4 (P2X4) (ATP receptor) (Purinergic receptor)	P2RX4	0.65	1.94E-02
Q01628	Interferon-induced transmembrane protein 3	IFITM3	0.65	1.81E-02
Q96SL1	Solute carrier family 49 member 4	SLC49A4	0.65	1.82E-02
Q8N4L2	Type 2 phosphatidylinositol 4.5-bisphosphate 4-phosphatase (Type 2 PtdIns-4.5-P2 4-Ptase)	PIP4P2	0.67	3.08E-06
P01130	Low-density lipoprotein receptor	LDLR	0.67	1.95E-06
P02511	Alpha-crystallin B chain	CRYAB	0.69	4.47E-02
P61916	NPC intracellular cholesterol transporter 2	NPC2	0.70	8.44E-06
P08962	CD63 antigen(Granulophysin) (Lysosomal-associated membrane protein 3) (LAMP-3)	CD63	0.72	3.98E-02
Q8IWE5	Pleckstrin homology domain-containing family M member 2	PLEKHM2	0.75	3.40E-02
P51159	Ras-related protein Rab-27A (Rab-27)	RAB27A	0.75	3.35E-03
Q13510	Acid ceramidase	ASAH1	0.76	3.60E-02
P11279	Lysosome-associated membrane glycoprotein 1 (LAMP-1)	LAMP1	1.37	2.91E-02
Q9UBR2	Cathepsin Z	CTSZ	1.44	2.85E-03
Q9NQX7	Integral membrane protein 2C	ITM2C	1.64	6.02E-03
P08195	Amino acid transporter heavy chain SLC3A2	SLC3A2	1.65	6.37E-05
Q01650	Large neutral amino acids transporter small subunit 1	SLC7A5	2.11	5.21E-03
P53634	Dipeptidyl peptidase 1	CTSC	2.65	1.90E-04

Modulated lysosomal and lysosomal-related proteins resulted from proteomic analysis of dermal fibroblasts derived from PD patients mutated in *TMEM175* gene compared to controls.

Pearson correlations of $r > |0.6|$. A cluster of coregulated features strongly relevant to the latent components of the multi-omics dataset was identified, which might be a potential characteristic of TMEM175 mutation (Fig. 12c, f).

The TMEM175 sample group gave a topological network (Fig. 12c) centred around 13 proteins (Rho GTPase-activating protein 24 (RHG24), Peptidyl-glycine alpha-amidating monooxygenase (AMD), Galectin-3 (LEG3), rRNA methyltransferase 1 mitochondrial (MRM1), V-type proton ATPase subunit H (VATH), Mannosyl-oligosaccharide 1,2-alpha-mannosidase (MA1C1), Endoplasmin (ENPL), Fibrillin-2 (FBN2), Tetratricopeptide repeat protein 38 (TTC38), Type 2 phosphatidylinositol 4,5-bisphosphate 4-phosphatase (PP4P2), E3 ubiquitin-protein ligase TRIM22 (TRI22), Beta-mannosidase (MANBA), LisH domain-containing protein ARMC9 (ARMC9), Ferritin heavy chain (FRIH), Membralin (MBRL), Lysosomal phospholipase A and acyltransferase (PAG15), Scinderin (SCIN), and Alpha- and gamma-adaptin-binding protein p34 (AAGAB)) mainly involved in biosynthetic processes which were positively correlated with PC and Cer species (Fig. 12c and Table 3). Interestingly, Insulin-like growth factor-binding protein 3 (IBP-3) and Argininosuccinate synthase (ASSY) were the only ones that presented exclusive negative correlation with PC species. In addition, a separate subnetwork emerged which was centred around Retinaldehyde dehydrogenase 3 (AL1A3), Carbonyl reductase [NADPH] 1 (CRB1), and Methylmalonic aciduria type A protein mitochondrial (MMAA). In this network all the proteins were positively correlated with PE and HexCer (Fig. 12c and Table 3).

The network analysis performed on PD_NoTMEM175-derived fibroblast cells (Fig. 12f) showed the presence of a cluster of PC and Cer classes positively correlated with six proteins: HLA class I histocompatibility antigen A alpha chain (HLAA), E3 ubiquitin-protein ligase TRIM22 (TRI22), V-type proton ATPase subunit H (VATH), Beta-adducin (ADDB), Interleukin-17 receptor A (I17RA) and Collagen alpha-1(XVIII) chain (COLA1). Endoplasmin (ENPL) was the only one negatively

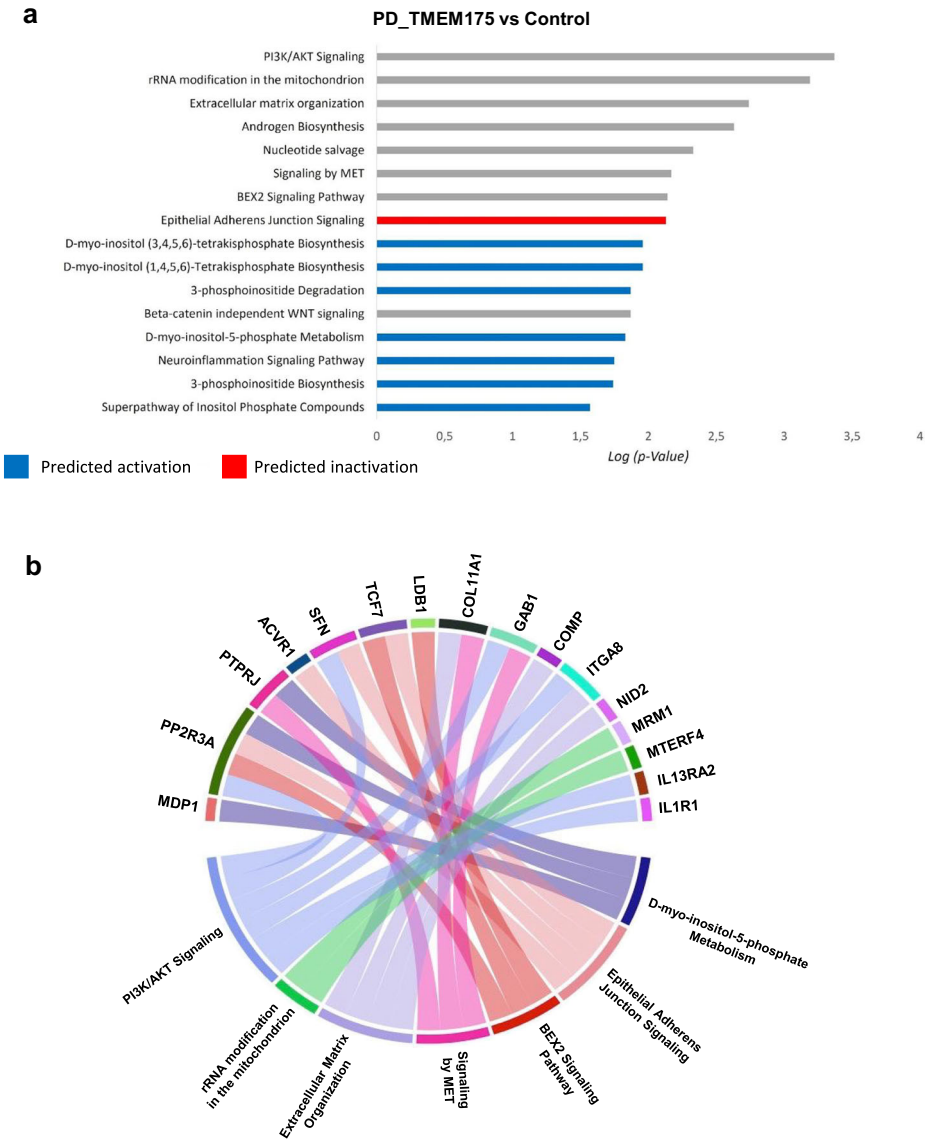

Fig. 11 | PD_TMEM175 group displayed alteration of lysosomal and mitochondrial proteins. **a** Complete list of canonical pathways associated with the dysregulated proteins identified in the respective dataset. *Y*-axis lists the canonical pathway, and the *X*-axis is the log of the corresponding *p*-value for each. Red colouring indicates the pathway is activated and blue colouring indicates the pathway is inhibited. No colouring indicates insufficient data in the dataset or the IPA knowledge base to determine if the pathway is activated or inhibited. **b** Graphical representation of cellular pathways and respective proteins resulted altered in PD_TMEM175-derived dermal fibroblasts compared to the controls.

correlated with PC and Cer (Fig. 12f). A separate subnetwork of PS, PI and PG classes was centred around two (Dynamin-1 (DYN1) and Probable cysteine--tRNA ligase mitochondrial (SYCM)) and three proteins (Semaphorin-7A (SEM7A), Na(+)/H(+) exchange regulatory cofactor NHE-RF2 (NHRF2) and Breast cancer anti-estrogen resistance protein 3 (BCAR3)) that were positively and negatively correlated, respectively (Fig. 12f).

Although this integrative analysis provided a set of multi-omics signatures for distinguishing the impact of TMEM175 mutation in patient-derived fibroblasts and revealed correlations between proteins and lipids within each group of analysis, these data need to be further validated on a larger cohort and functional interpretation is speculative.

Discussion

This is the first study that adopted an untargeted omics approach to disclose potential lipidomic, metabolomic and proteomic alterations in PD patients carrying *TMEM175* mutation.

We focused our study on *TMEM175* which encodes for an endo-lysosomal ion channel playing an important role in maintaining lysosomal pH and in regulating lysosomal functioning[14,28]. Recently, *TMEM175* was also described as an important PD risk factor[10,29–32] and we found that mutations occurring in this gene affected about 8% of the Italian PD cohort[11]. In order to evidence all metabolic alterations due to the presence of *TMEM175* mutations at both circulating and cellular level, we stratified our PD cohort into two subgroups based on the presence or absence of mutation in this gene. The analysis of the lipidomic profile revealed a wide dysregulation in the most of lipid classes in both groups of PD patients compared to the controls. In PD_TMEM175 patients we observed a significant dysregulation of many lipid classes closely related to lysosome and mitochondria metabolism including Acylcarnitines (CAR), Ceramides (Cer), Fatty Acids (FA), Hexosylceramide (HexCer), Phosphatidylcholines (PC), Ether-linked Phosphatidylcholine (PC O-), Lysophosphatidylcholines (LPC), Sphingomyelin (SM) and Phosphatidylinositol (PI) at both cellular and plasma level.

Acylcarnitines were increased at cellular and circulating level, mainly in PD-TMEM175 group, suggesting a dysregulation of their metabolism in these patients. Based on their chain, Acylcarnitines are classified into four subgroups: short-chain, medium-chain, long-chain and very long-chain. Previous studies reported decreased level of long-chain Acylcarnitine in the serum of PD patients[33], whereas, in our study, we observed a significant wide increase affecting all the four subgroups of Acylcarnitines detected in the plasma of TMEM175 patients. In these patients, six CAR lipids such as CAR 16:0, CAR 16:1, CAR 16:2, CAR 18:2, CAR 18:3, CAR 20:4, among all the Acylcarnitines deregulated species, were significantly increased both in plasma and in cells. The most important function of Acylcarnitines is to support long fatty-acid β-oxidation and provide energy for cellular

Table 3 | Integration analysis of lipidomic and proteomic data in fibroblasts revealed a group of proteins correlated to PC, Cer, PE and HexCer in PD_TMEM175 group

Entry	Entry name	Protein	Pathway
Proteins positively correlated to PC and Cer—Cluster 1			
Q8N264	RHG24_HUMAN	Rho GTPase-activating protein 24	Signal transduction
P19021	AMD_HUMAN	Peptidyl-glycine alpha-amidating monooxygenase	Fatty acid primary amide biosynthetic process
P17931	LEG3_HUMAN	Galectin-3 (Gal-3) (Carbohydrate-binding protein 35)	Innate immune response
Q6IN84	MRM1_HUMAN	rRNA methyltransferase 1. mitochondrial	rRNA modification
Q9UI12	VATH_HUMAN	V-type proton ATPase subunit H (V-ATPase subunit H)	Golgi lumen acidification; intracellular pH reduction; lysosomal lumen acidification
Q9NR34	MA1C1_HUMAN	Mannosyl-oligosaccharide 1.2-alpha-mannosidase IC	Carbohydrate metabolic process
P14625	ENPL_HUMAN	Endoplasmin (glucose-regulated protein)	Cellular response to ATP; negative regulation of apoptotic process; protein folding in endoplasmic reticulum; response to endoplasmic reticulum stress
Q8N4L2	PP4P2_HUMAN	Type 2 phosphatidylinositol 4.5-bisphosphate 4-phosphatase	Phosphatidylinositol dephosphorylation
Q8IYM9	TRI22_HUMAN	E3 ubiquitin-protein ligase TRIM22	Positive regulation of autophagy
O00462	MANBA_HUMAN	Beta-mannosidase (Lysosomal beta A mannosidase)	Glycoprotein catabolic process; oligosaccharide catabolic process; protein modification process
P02794	FRIH_HUMAN	Ferritin heavy chain	Intracellular sequestering of iron ion; iron ion transport; negative regulation of cell population proliferation
Proteins negatively correlated to PC—Cluster 1			
Q8NCC3	PAG15_HUMAN	Lysosomal phospholipase A and acyltransferase	Ceramide metabolic process; diacylglycerol biosynthetic process; fatty acid catabolic process; glycerophospholipid metabolic process
P17936	IBP3_HUMAN	Insulin-like growth factor-binding protein 3 (IBP-3)	Apoptotic process; positive regulation of insulin-like growth factor receptor signalling pathway [GO:0043568]; positive regulation of MAPK cascade; regulation of glucose metabolic process
Proteins positively correlated to PE and HexCer—Cluster2			
P47895	AL1A3_HUMAN	Retinaldehyde dehydrogenase 3 (RALDH-3) (Aldehyde dehydrogenase 6)	Apoptotic process
P16152	CBR1_HUMAN	Carbonyl reductase [NADPH] 1	Cyclooxygenase pathway; positive regulation of reactive oxygen species metabolic process

List of proteins detected in topological network 1 and 2 resulted from integrative analysis. Entry: UniProt id; Entry name: the name of the protein reported in UniProt (https://www.uniprot.org/). Pathways reported were adapted from Gene Ontology in terms of cellular process.

processes[34]. Their deregulation could lead to an impairment in energy production and mitochondrial functioning. It is interesting to note that impairment in mitochondrial functioning is also present in cellular model knock-out for TMEM175[13].

An interesting finding of this study is the significant increase, in the plasma of TMEM175 patients, of endo-lysosomal sphingolipids such as Cer, HexCer and SM. HexCer is also increased in dermal fibroblasts as also described in patients carrying GBA mutations[17]. In fact, Cer, HexCer and SM molecules are all affected by impaired GCase activity, underlying the interrelated nature of sphingolipid metabolism and suggesting that TMEM175 mutations, affecting lysosome pH and metabolism, could lead to an initial GCase impairment ultimately altering the function of other enzymes, such as α-sphingomyelinase and ceramide synthases (CerS), involved in this metabolism[11,35,36].

Increased oxidative stress is a central event in neuronal failure that induces the activation of the sphingomyelin (SM)-ceramide pathway, making them key players in neurodegeneration. Sphingomyelins were previously described as structural components of cell membranes and involved in apoptosis, autophagy, and immune response[37–39]. Some lipids of this class were increased in the anterior cingulate cortex[40], in the primary visual cortex and in the Substantia Nigra of male PD patients[41]. Ceramide has been proposed to be a second messenger in diverse cellular signalling pathways, with levels of ceramides being transiently altered by several extracellular signals and physiological changes[37]. Several publications reported altered levels of both ceramides and sphingomyelins in patients affected by neurodegenerative disorders including PD, Alzheimer's disease (AD), multiple sclerosis (MS) and dementia with Lewy bodies (DLB)[42]. This is the first study that describes a significant dysregulation of these lipid classes in a well-stratified cohort of patients, carrying specific gene mutations, both in cells and circulating biofluid.

Phosphatidylcholines (PCs) represent the most abundant lipids in the cells because they are the major components of all cellular membranes, and they play a crucial role in lipoprotein formation and stability[43]. PCs have been demonstrated to be part of lipid droplets' surface, and are important in regulating their dynamics. Lipid droplets are important players in crucial events for cellular physiology including cellular lipotoxicity and de novo lipogenesis[44]. Several studies described an alteration of PC at circulating levels in PD patients with contrasting results and without considering the presence of specific genetic mutations[45–47]. It is interesting to highlight that in our study, the group of PD patients carrying TMEM175 mutation exhibits a significant increase of PC in plasma with respect to PD_NoTMEM175 patients and to controls suggesting that genetic background could influence PC metabolism. Instead, the data obtained in dermal fibroblasts need to be taken with caution and require further validation in a larger cohort. Recent studies suggested that changes in PC levels could be the consequence of alpha-synuclein (αS) accumulation on membranes, as also observed in yeast and rat cortical neuron models of αS excess[48]. Moreover, in PD patients carrying TMEM175 mutation, we disclosed a significant correlation between the concentration in plasma of PC with age and with an earlier age at the onset of the disease.

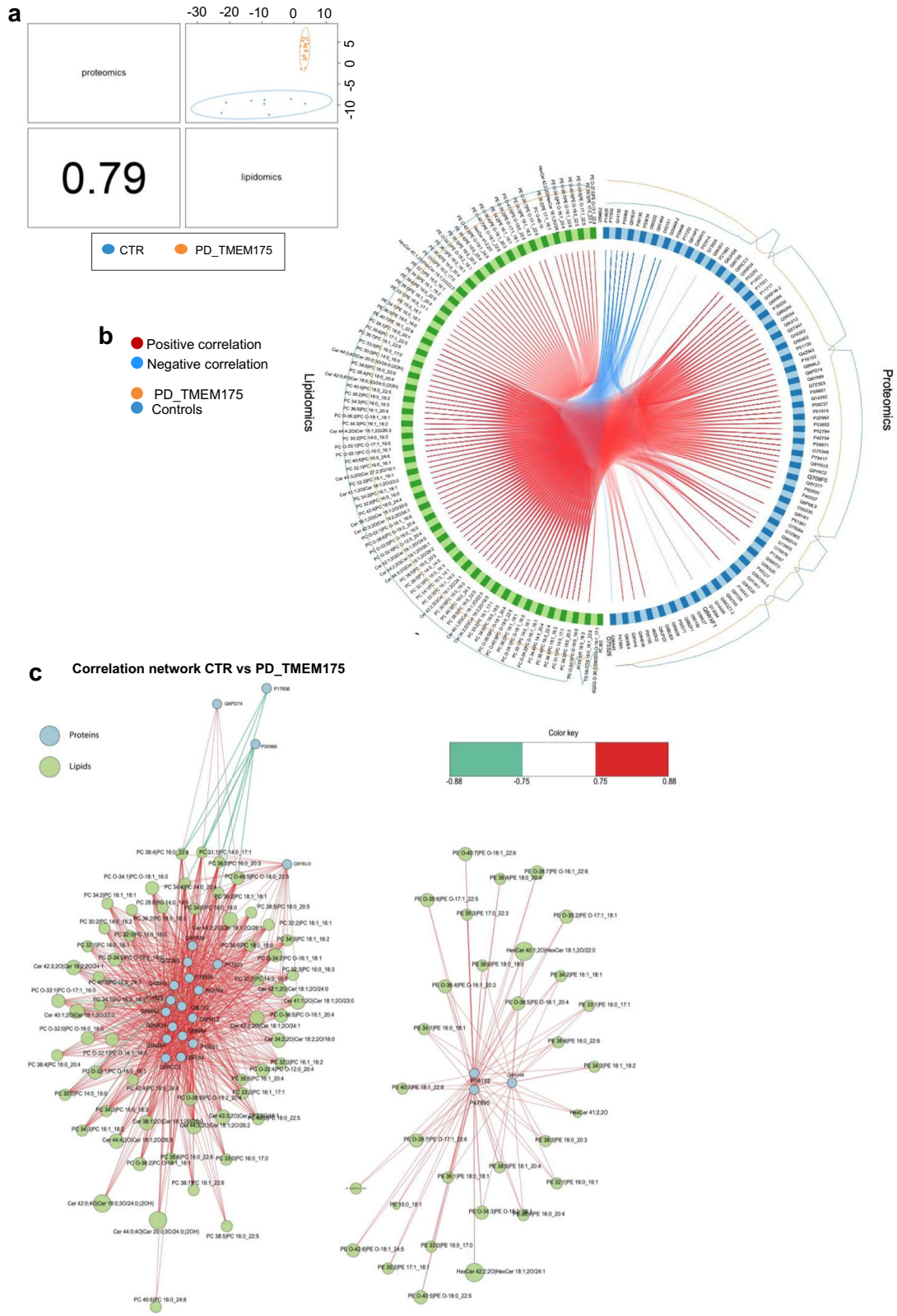

Fig. 12 | Integrative correlation analysis of proteome and lipidome of PD_TMEM175 cellular models. Comprehensive exploration with data integration analysis of proteomics and lipidomics data from cellular models. **a**, **d** Inter-omics correlations presented by sample scatterplots displaying the first components of each dataset (proteins and lipids) when comparing both PD_TMEM175 (**a**) and PD_NoTMEM175 groups (**d**) with respect to controls. Correlations were calculated using Pearson correlation between each dataset (lower diagonal plot). **b**, **e** Circos plot representing the averaged expression of proteins and lipids in each cell type (PD_TMEM175 and PD_NoTMEM175) and correlations between the features selected in each of the data blocks (protein features coloured in blue, and lipids features in green). **c**, **f** Relevant network plot showing positive (red lines) and negative (green lines) correlations between features from each dataset.

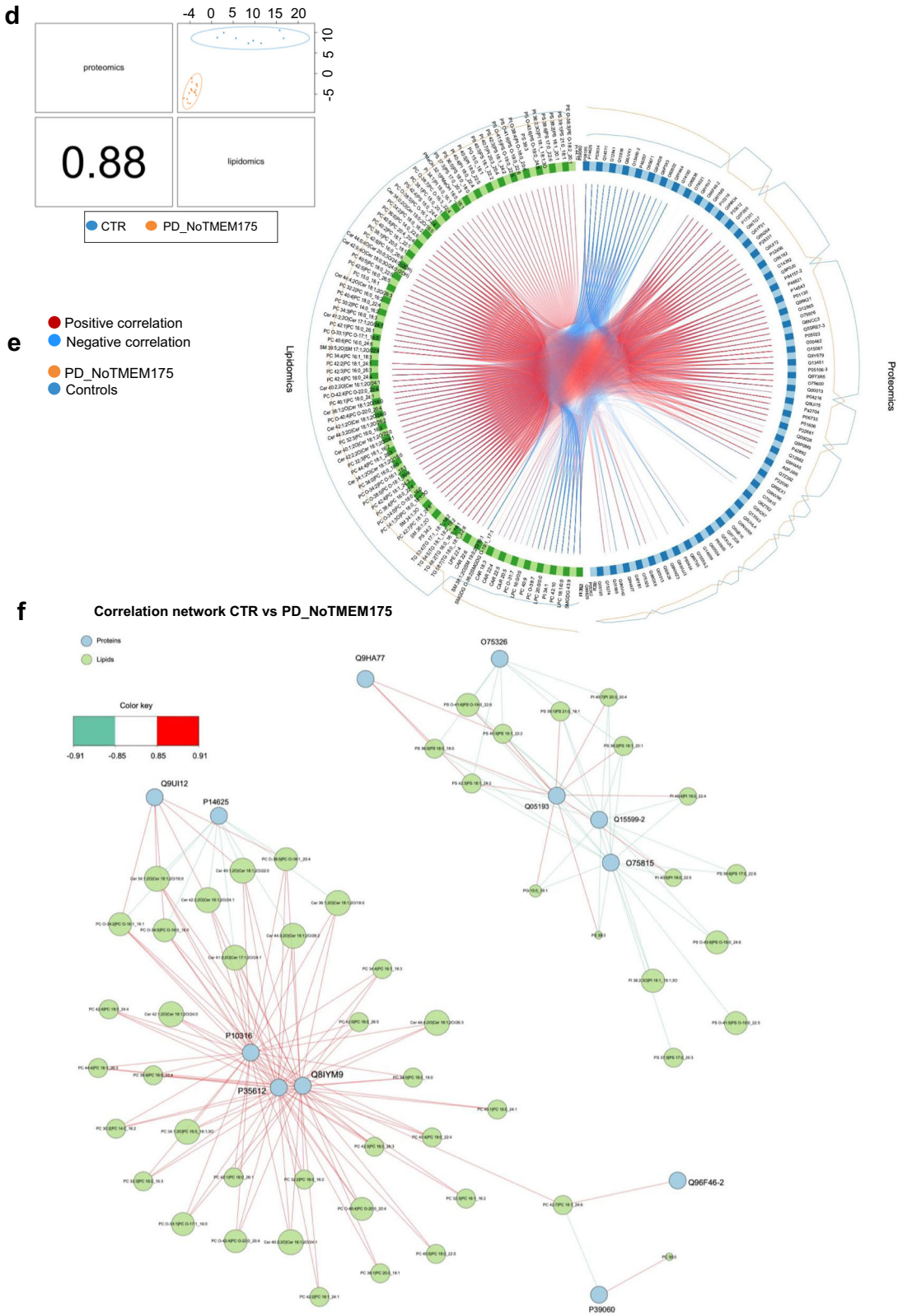

Of great interest is the finding that the levels of Phosphatidylinositol (PI) were significantly increased both in plasma and in fibroblasts of PD patients carrying TMEM175 mutations. PIs are a relevant component of cell membranes[49] and are an important player in cellular signal transduction[50]; their role in PD etiopathogenesis is still not elucidated. Controversial results described elevated levels of PI 34:1 in Parkin-mutant skin fibroblasts[16], while decreased levels of the entire PI lipid class were observed in the SN of male PD patients[51]. In our cohort, we found that among the most dysregulated lipid species, PI 34:1|PI 16:0_18:1 was the only lipid showing a significant correlation ($r = -0.55$; $p = 0.006$) with the age and with an earlier age at onset of motor symptoms only in patients carrying TMEM175 mutations.

Metabolomics analysis performed in plasma identified among the most enriched and impacted pathways discovered by KEGG database analysis, those related to amino acid metabolism such as tryptophan metabolism, lysine degradation, alanine, aspartate, and glutamate metabolism. The most significant altered metabolites in these pathways were L-threonine, L-tyrosine, L-aspartate, L-glutamine, L-asparagine, L-lysine, L-glutamate, L-tryptophan, meanly increased in PD_NoTMEM175 patients suggesting a completely different energy metabolism into the two groups of patients.

Changes in glutamic acid concentrations seem to be of interest, as this amino acid plays a role as a neurotransmitter in the brain and is involved in the pathogenesis of PD and development of LID[52]. In our cohort, we observed a reduction, although non-significant, of plasma levels of L-Glutamate in PD TMEM175 patients and a significant increase in PD No_TMEM175 patients. However, we observed a strongly significant correlation with the severity of motor and non-motor symptoms in PD TMEM175 patients. In literature, conflicting results have been reported on L-Glutamate levels and PD pathology[53–55], while significant negative correlation between glutamate concentration and duration of the disease has been suggested[56]. Some authors reported that increased serum concentrations of glutamate may reflect increased cerebral glutamatergic activity[57,58]. Moreover, there is evidence that glutamatergic overactivity is a critical mechanism underlying different PD-associated striatal alterations in early and advanced symptomatic stages of the disease[59]. Additional data on a larger cohort could be useful to fully elucidate the role of Glutamate on PD occurrence and severity.

The analysis of proteomic composition conducted in dermal fibroblasts derived from both PD patients and controls revealed a wide deregulation of lysosome, autophagy and mitochondrial pathways in PD patients carrying TMEM175 mutations, supporting a relevant role of this channel in regulating these cellular processes. We discovered significant decreased amount of several key enzymes working at lysosome, autophagosome, endoplasmic reticulum (ER), and plasma membrane, including PAG15, PP4P1, GALC, FYV1, PIGO, PGPS1 and PLPP1 involved in phosphosphingolipids (SM) and glycerophospholipids (PC, PG, PI etc.) biosynthetic pathways in the group of PD_TMEM175 patients. These data might potentially confirm the presence of an altered lipid metabolism at cellular level, which could mirror an upregulation of lipids observed at circulating and cellular level[19].

Galactosyl ceramidase (GALC) is a lysosomal enzyme involved in sphingolipid metabolism by removing β-galactose from β-galactosylceramide[60]. Genome-wide association studies have revealed the GALC locus on chromosome 14 associated with PD[28,61,62]. Recently it has been demonstrated that GALC is the gene associated with PD in this locus and that associated variants in GALC increased galactosyl ceramidase expression and activity[61].

PP4P1, FYV1 and PIGO are involved in Phosphatidylinositol metabolism. PP4P1 catalyses the hydrolysis of phosphatidylinositol-4,5-bisphosphate (PtdIns-4,5-P2) to phosphatidylinositol-4-phosphate (PtdIns-4-P). It regulates lysosomal positioning by recruiting JIP4 to lysosomal membranes, thus inducing retrograde transport of lysosomes along microtubules[63]. Moreover, it also contributes to the assembly of the V-ATPase complex in lipid rafts of the lysosomal membrane and to subsequent amino acid-dependent activation of mTORC1[64]. FYV1 catalyses the phosphorylation of phosphatidylinositol 3-phosphate to form PtdIns(3,5)P2[65]. This kinase is implicated in myriad essential cellular processes such as the maintenance of endomembrane homoeostasis, and endocytic-vacuolar pathway, lysosomal trafficking, nuclear transport, stress- or hormone-induced signalling and cell cycle progression[66]. These findings were also supported by Ingenuity Pathway Analysis which discovered a significant deregulation of proteins involved in D-myo-inositol-5-phosphate synthesis and metabolism. Myo-inositol is crucial for producing phosphoinositides which are described to be able to interact with α-synuclein[23–26]. Recently, the group of Dickson elucidated a mechanism by which PM PI(4,5)P2 dysregulation caused neuronal cell death and that normalisation of PM PI(4,5)P2 levels resulted in reduced a-Syn aggregates and in the rescue of neuron viability in PD models[67]. Our study reported the first evidence of a significant association between a specific lipid specie (PI 34:1|PI 16:0_18:1), belonging to the PI lipid class, and the presence of *TMEM175* mutations in PD patients as well as an earlier age at the onset of the disease in this group of patients. These data were also supported by a significant alteration of enzymes involved in PI metabolism observed in PD TMEM175 patients. Additional studies are necessary to highlight a possible mechanism of regulation between phosphoinositides and TMEM175 activity.

Lysosomal Phospholipase A2 (PAG15) is a lysosomal enzyme which hydrolyses lysophosphatidylcholine to glycerophosphorylcholine and a free fatty acid. Phosphatidylglycerophosphate Synthase 1 (PGPS1) is responsible for producing Glycerophosphoglycerols (PG) lipid class mainly into mitochondria, which represented the precursor for cardiolipin and bis(monoacylglycerol)phosphate (BMP) synthesis in lysosomes and mitochondria respectively[19].

Phospholipid Phosphatase 1 (PLPP1) converts phosphatidic acid to diacylglycerol, and functions in the synthesis of glycolipids and in phospholipase D-mediated signal transduction. This enzyme is an integral membrane glycoprotein that plays a role in the hydrolysis and uptake of lipids from extracellular space (including S1P)[68].

Interestingly, the analysis also reflected an alteration of proteins involved in the insulin pathway including AHSG, ALB, C3, ITIH2, SERPINC1, IF2B1, MPRI, GLUT-6 and GLUT-10. Past evidence has described that impairment of insulin signalling has been found to increase the risk of AD[69,70] and PD[71,72] indicating a possible link between Insulin pathway regulation and neurodegenerative diseases. Moreover, it was noted that the pathway of Insulin growth factor regulates the activation of PI3K/Akt signalling which is also important for regulating neuronal survival and synaptic plasticity during ageing and many neurodegenerative diseases[73]. It is interesting to remark that this pathway was discovered by IPA as significantly modulated in PD patients carrying TMEM175 mutations and that several mutations identified in this gene affected the binding between AKT and TMEM175 channel[11].

Among modulated lysosomal proteins, SPHM and SNX14 are particularly intriguing since their downregulation is much more significant in the comparison between TMEM175 group and controls with respect to non-mutated group and controls. The deficiency of these proteins is reported to be linked to lysosome storage disorders and neurodegeneration: SPHM is involved in heparan sulfate degradation in lysosomes[74]. Mutation-driven deficiency of this protein provokes heparan sulfate accumulation and results in Sanfilippo A syndrome, which is characterised by central nervous system's aberrations[75]. SNX14 acts in synaptic signalling and might have a role in the fusion between autophagosome and lysosome[76]. Mutations in SNX14 gene are related to cerebellar atrophy in paediatric onset ataxias[76] and in cerebellar neurodegenerative pathologies[77]. In particular, SNX14 deficiency is linked to lipid dysregulation during neurodegeneration, characterised by a strong increase in acylcarnitine[77]. Strikingly, in our data, we have also found an increase in this class of lipids, especially in TMEM175 group, with respect to controls, highlighting crosstalk between protein and lipid impairment in patients' derived fibroblasts.

We also discovered a significant downregulation of enzymes implicated in numerous finely regulated mitochondrial processes, such as mitochondrial translation, ATP biosynthetic process, mitochondrial organisation, and response to oxidative stress. Interestingly, we found a downregulation of several proteins including the Acyl-CoA dehydrogenase family members 10 and 11 (ACD10 and ACD11) and the Short-chain specific acyl-CoA dehydrogenase (ACADS), involved in fatty acid beta-oxidation and degradation. These findings, together with altered levels of acylcarnitine might suggest that TMEM175 mutations might have an impact also on mitochondria metabolism.

Integration analysis of lipidomic and proteomic data in dermal fibroblasts discovered, in TMEM175 patients, two clusters of proteins correlated with PC and CER and with PE and HexCer, respectively. The identified

proteins are involved in the metabolic pathways of Glycerophospholipids, Fatty acids and Sphingolipids (PP4P2, AMD and PAG15), in the autophagy (TRIMM22), in lysosome functioning (ATP6V1A and MANBA) and in glucose metabolism such as Endoplasmin and Insulin-like growth factor-binding protein 3 (IBP-3). A positive correlation was also observed with Galectin-3 (GAL3), a β-galactoside-binding cytosolic lectin, that unifies and coordinates ESCRT and autophagy responses to lysosomal damage[78]. In neuronal cells, GAL3 interacts with endogenous αSyn fibrils and affects spatial propagation and the stability of pre-formed αSyn fibrils resulting in short, amorphous toxic strains[79].

The study presents several limitations, which include the size of the study sample, the lack of proteomic analysis in plasma, which does not allow us to study the presence of lipid and protein interactions in biofluids as well as the lack of data related to plasma lipoprotein levels. Moreover, in this study, untargeted lipidomic analysis did not reveal several specific lysosomal lipids, such as glucosylsphingosine and BMP, in plasma samples. To quantify these lipids targeted analysis should be integrated. Although our data need further validation in a wide number of patients, this study highlights novel pathways related to PD and mutation in TMEM175 gene. Overall, these results might serve as the basis for the development of future testable hypotheses. Moreover, the study supports the hypothesis that the stratification of patients might help in the detection of slight differences that could be lost by analysing large cohorts with high genetic heterogeneity.

Methods

PD cohort population

804 independent and unrelated PD patients (501 males; 300 familiar and 504 sporadic cases) were recruited at the IRCCS Mediterranean Neurological Institute (MNI) in Pozzilli. All PD subjects were of European ancestry and were evaluated by neurologists of the Parkinson Study Group, according to published diagnostic criteria[80]. The PD cohort was recruited from June 2015 to December 2017, and from June 2021 to December 2022, with a thorough protocol comprising neurological examination and evaluation of non-motor domains. All the PD patients were of European ancestry and information about family history, demographic characteristics, anamnesis, and pharmacological therapy was also collected. The Movement Disorder Society revised version of the Unified Parkinson's Disease Rating Scale Part III (33 items, maximum score 132; hereafter called UPDRS) was used to assess clinical motor symptoms. These included language, facial expressions, tremor, rigidity, agility in movements, stability, gait and bradykinesia. Cognitive abilities were tested through an Italian validated version of the Montreal Cognitive Assessment (MoCA). Cognitive domains assessed include short-term memory (5 points); visuospatial abilities via clock drawing (3 points), and a cube copy task (1 point); executive functioning via an adaptation of Trail Making Test Part B (1 point), phonemic fluency (1 point), and verbal abstraction (2 points); attention, concentration, and working memory via target detection (1 point), serial subtraction (2 points), digits forward and backward (1 point each); language via confrontation naming with low-familiarity animals (3 points), and repetition of complex sentences (2 points); and orientation to time and place (6 points). The total score was given by the sum of these domains and then divided by the maximum score that could be obtained (30 points). Non-motor symptoms were assessed through an Italian validated version of Non Motor Symptoms Scale (NMS) for Parkinson Disease. This scale tests 9 items, including cardiovascular domain, sleep/fatigue, mood/cognition, perceptual problems/hallucinations, attention/memory, gastrointestinal, urinary, sexual function, and ability to taste or smell. The 804 PD patients, additionally with 282 healthy subjects, were analysed by Whole Exome Sequencing (WES). Among the 804 PD patients, we found 63 PD patients carrying mutations in TMEM175 gene.

All procedures involving human participants were approved by the Institutional Review Board of IRCCS Neuromed. Approved study protocols: N°9/2015, N°19/2020 and N°4/2023; Clinicaltrials.gov registrations: NCT02403765, NCT04620980, NCT05721911. Clinical investigations were conducted according to the principles expressed in the Declaration of Helsinki. Written informed consent was obtained from all participants.

Human dermal fibroblasts hDF cell line

For lipidomic and proteomic analysis at cellular level, we utilised human dermal fibroblasts (hDF) from a selected cohort of PD patients (PD_TMEM175 ($N = 6$), PD_NoTMEM175 ($N = 4$)) and controls ($N = 2$). The hDF cells were generated in our laboratory. Skin samples of PD patients and unrelated healthy individuals were obtained by punch biopsy mostly at the inner side of the upper arm. Tissue pieces were enzymatically digested for 5 h at 37 °C by using Collagenase/Dispase kit (Roche Diagnostics, Mannheim, Germany), followed by mechanical disaggregation with a knife. Cells were grown in Dulbecco's modified Eagle's medium (DMEM) supplemented with 4.5 g/L D-glucose, 0.11 g/L sodium pyruvate, 20% FBS, 1% NEAA, 1% L-glutamine, and 1% Pen-Strep at 37 °C in a humidified CO_2 5% air for about 4–5 weeks. hDF cell lines were maintained and were used in all the experiments in sub-confluent monolayers. Starvation was performed for 1 h in HBSS.

Sample preparation

Blood samples from PD patients and healthy subjects were collected in blood collection tubes (BD Vacutainer, K2E (EDTA)) then, after two centrifugations at 1900×*g* for 10 min, plasma was aliquoted and stored at −80°. Unique anonymized codes have been assigned to the samples for processing and subsequent analysis, maintaining the confidentiality of personal data. The extraction of plasma lipids was carried out with a biphasic method: 30 µL of plasma was introduced into a tube and extracted with 225 µL of cold MeOH containing a combination of deuterated standards (Splash Lipidomix®). The solution was then vortexed for 10 s, and 750 µL of cold MTBE was added and vortexed for 10 s. The tube was then placed in a thermomixer at 4 °C and vortexed for 6 min at 2000 rpm. After that, 188 µL of water was added, and the tube was vortexed for 10 s and then centrifuged for 2 min at 14,000 rpm at 4 °C. Finally, 300 µL of supernatant was collected and evaporated with a SpeedVac. The dried sample was replenished with 50 µL of a 9:1 MeOH/toluene solution containing the internal standard CUDA (12.5 ng/mL). For lipidomic analysis, cells were extracted using 1 mL of 75:15 IPA/H2O solution, after the addition of 100 µL of CH_3OH 5% deuterated standard (Splash Lipidomix®). Then the samples were vortexed for 30 s, sonicated for 2 min, vortexed again for 30 s and then they were incubated for 30 min at 4 °C, under gentle, constant shaking. Subsequently, samples were rested on ice for an additional 30 min. To remove debris and other impurities, the samples were centrifuged for 10 min at 3500×*g* at 4 °C. 1 mL of supernatant was collected and dried using a SpeedVac centrifuge (Labogene). The dried samples were reconstituted in 100 µL of CH_3OH containing the internal standard CUDA (12.5 ng/mL). For proteomic analysis, cells were lysed with RIPA buffer and sonicated. Proteins were then precipitated with cold acetone and resuspended. Proteins were then reduced in 25 µL of 100 mM NH_4HCO_3 with 2.5 µL of 200 mM DTT (Merck) at 60 °C for 45 min and next alkylated with 10 µL 200 mM iodoacetamide (Merck) for 1 h at RT in dark conditions. Iodoacetamide excess was removed by the addition of 200 mM DTT. Proteins were then digested with trypsin. The digests were dried by Speed Vacuum and then desalted[81].

Metabolites were extracted as reported by Barberis et al.[82]. Briefly, 500 µL of an ACN/IPA/water (3:3:2) solution, with tridecanoic acid at 1 ppm as internal standard, was added to 12 µL of plasma. After vertexing, the sample was centrifuged at room temperature for 15 min at 14,500×*g*. The supernatant was then dried in a speed-vacuum. The sample was derivatized with methoximation (20 µL of Methoxamine, 80 °C, 20 min) and underwent sialylation (90 µL of BSTFA, 80 °C, 20 min). After this, 10 µL of hexadecane (IS) were added to the sample before the GCxGC-MS analysis.

Lipidomic analysis

For lipidomic analysis, reconstituted samples were analysed with a Vanquish UHPLC system (Thermo Scientific, Rodano, Italy) coupled with an Orbitrap Q-Exactive Plus (Thermo Scientific, Rodano, Italy). Lipid

separation was performed using a reversed-phase column (Hypersil Gold™ 150 × 2.1 mm, particle size 1.9 µm) maintained at 45 °C with a flow rate of 0.260 mL/min. Mobile phase A for ESI mode positive consisted of 60:40 (v/v) acetonitrile/water with ammonium formate (10 mmol) and 0.1% formic acid, while mobile phase B was 90:10 isopropanol/acetonitrile (v/v) with ammonium formate (10 mmol) and 0.1% formic acid, while in the negative ESI mode, the organic solvents for both mobile phases were the same as in the positive with the exception of using ammonium acetate (10 mmol) as a mobile phase modifier. The gradient used was as follows: 0–2 min from 30 to 43% B, 2–2.1 min from 43 to 55% B, 2.1–12 min from 55 to 65% B, 12–18 min at 65% to 85% B, 18–20 min at 85% to 100% B; 100% B was held for 5 min, and then the column was allowed to equilibrate to 30% B for another 5 min. The total running time was 30 min. Mass spectrometry analysis was performed in both positive ion (at 3.5 kV) and negative ion (2.8 kV) modes. Data were collected in a data-dependent top 10 scan mode (ddMS2). MS full-scan survey spectra (mass range m/z 80–1200) were acquired with a resolution of R = 70,000 and target AGC of 1 × 106. MS/MS fragmentation was performed using high energy c-trap dissociation (HCD) with R = 17,500 resolution and 1 × 105 AGC target. The step normalised collision energy (NCE) was set to 15, 30 and 45. The injection volume was 3 µL. For accurate mass-based analysis, regular Lockmass and interrun calibrations were used. An exclusion list for background ions was generated by testing the same procedural sample for both positive and negative ESI modes22. Quality control was ensured by analysing pooled samples before, at the beginning and at the end of the batches; using blanks to check for residual interference; and using internal standards, directly in plasma or cell samples, which include a series of analyte classes at levels appropriate for the plasma (Avanti SPLASH Lipidomix) and an internal standard (CUDA) prior to liquid chromatography-mass spectrometry (LC–MS) analysis.

Raw data acquired from lipidomic untargeted analysis were processed with MSDIAL software (Yokohama City, Kanagawa, Japan), version 4.24. Peaks were detected, MS2 data were deconvoluted, compounds were identified, and peaks were aligned across all samples. For quantification, the peak areas for the different molecular species detected were normalised using the deuterated internal standard for each lipid class. To obtain an estimated concentration expressed in nmol/mL (plasma), the normalised areas were multiplied by the concentration of the internal standard. An in-house library of standards was also used for lipid identification.

Proteomic analysis

Digested peptides were analysed on an Ultimate 3000 RSLC nano coupled directly to an Orbitrap Exploris 480 with a High-Field Asymmetric Waveform Ion Mobility Spectrometry System (FAIMS) (all Thermo Fisher Scientific). Samples were injected onto a reversed-phase C18 column (15 cm × 75 µm i.d., Thermo Fisher Scientific) and eluted with a gradient of 6% to 95% mobile phase B over 41 min by applying a flow rate of 500 nL/min, followed by an equilibration with 6% mobile phase B for 1 min. The acquisition time of one sample was 41 min and the total recording of the MS spectra was carried out in positive resolution with a high voltage of 2500 V and the FAIMS interface in standard resolution, with a CV of −45V. The acquisition was performed in data-independent mode (DIA): precursor mass range was set between 400 and 900, isolation window of 8 m/z, window overlap of 1 m/z, HCD collision energy of 27%, orbitrap resolution of 30,000 and RF Lens at 50%. The normalised AGC target was set to 1000, the maximum injection time was 25 ms, and microscan was 1. For DIA data processing, DIA-NN (version 1.8.1) was used: the identification was performed with "library-free search" and "deep learning-based spectra, RTs and IMs prediction" enabled. Enzyme was set to Trypsin/P, precursors of charge state 1–4, peptide lengths 7–30 and precursor m/z 400–900 were considered with maximum two missed cleavages. Carbamidomethylation on C was set as fixed modification and Oxidation on M was set as variable modification, using a maximum of two variable modifications per peptide. FDR was set to 1%.

The mass spectrometry proteomics data have been deposited to the ProteomeXchange Consortium via the PRIDE partner repository with the dataset identifier PXD049990.

Metabolomic analysis

Metabolomics results were generated with a LECO Pegasus 4D Time-of-Flight Mass Spectrometer (Leco Corp., St. Josef, MI, USA) equipped with a LECO dual-stage quad jet thermal modulator. The GC part of the instrument was an Agilent 7890 gas chromatograph (Agilent Technologies, Palo Alto, CA, USA) equipped with a split/splitless injector. The first dimension column was a 30 m Rxi-5Sil (Restek Corp., Bellefonte, PA, USA) MS capillary column with an internal diameter of 0.25 mm and a stationary phase film thickness of 0.25 µm, and the second dimension chromatographic column was a 2 m Rxi-17Sil MS (Restek Corp., Bellefonte, PA, USA) with a diameter of 0.25 mm and a film thickness of 0.25 µm. High-purity helium (99.9999%) was used as the carrier gas, with a flow rate of 1.4 mL/min. One µL of the sample was injected in splitless mode at 250 °C. The temperature programme was as follows: the initial temperature was 100 °C for 2 min, then ramped 20 °C/min up to 330 °C and then held at this value for 2 min. The secondary column was maintained at +5 °C relative to the GC oven temperature of the first. Electron impact ionisation was applied (70 eV). The ion source temperature was set at 250 °C, the mass range was 25 to 550 m/z with an extraction frequency of 32 kHz. The acquisition rates were 200 spectra/s and the modulation period for the 2D analysis was 4 s for the entire run. The modulator temperature offset was set at +15 °C relative to the secondary oven temperature, while the transfer line was set at 280 °C.

The chromatograms were acquired in total ion current mode. Peaks with a signal-to-noise (S/N) value lower than 500.0 were rejected. ChromaTOF version 5.31 was used for the raw data processing. Mass spectral assignment was performed by matching with the NIST MS Search 2.3 libraries and the FiehnLib. An in-house library of standards was also used for the small molecules identification[83].

LECO ChromaTOF software was used for all acquisition control of metabolomics data, raw data processing and Statistical Compare for alignment of all analytes. The exported data were normalised for internal standards and optimised by lowess normalisation using quality control samples.

Statistical analysis

Clinical and demographic characteristics were described using, as summary statistics, median and the interquartile range (IQR) or absolute and relative frequencies. Comparisons between PD patients and CNT were evaluated using MedCalc statistical software for continuous variables and Chi-square test for dichotomous variables. Statistical analyses of lipidomic, proteomic and metabolomic samples were performed with MetaboAnalyst 6.0 (www.metaboanalyst.org). Statistical Analysis [single factor] function was used to build volcano plots, principal component analysis (PCA), partial least squares-discriminant analysis (PLS-DA) and heatmaps. Pathway and Enrichment analysis functions were performed to integrate pathway enrichment analysis and pathway topology analysis, starting from significant metabolites found in statistics. GraphPad Prism 8 was used for unpaired Student's *T*-test and ONE-way ANOVA statistical analysis.

Comparison of plasma lipids levels between PD and CNT was performed using unpaired *T*-test.

Linear regression analysis to compare lipids and metabolite concentrations with endophenotypes was performed with STATS.BLUE (https://stats.blue/Stats_Suite/correlation_regression_calculator.html). Significance was set at $p < 0.05$ for all analyses. Pearson's correlation analysis was carried out with GraphPad 8 and the resulting *p*-value was corrected with Bonferroni. Bioinformatic analysis was carried out using DAVID software (https://david.ncifcrf.gov/tools.jsp) and Ingenuity Pathway Analysis (Qiagen, Hilden, Germany).

Integrative multi-omics analysis

To identify the highly correlated features discriminating TMEM mutation, we performed Data Integration Analysis for Biomarker discovery using Latent cOmponent (DIABLO)[27] analysis of proteomic and lipidomic data of dermal fibroblasts of PD patients carrying mutations in TMEM175 and with no TMEM175 mutation. Dimension reduction was performed with an

information gain algorithm to obtain only significant features among each group using proteomic and lipidomic data separately. The DIABLO R software was used to separately analyse each combination, utilising the (MixOmics) library. The sPLSDA model was employed to determine the correlation between the proteomic and lipidomic data for each group. The model was constructed using a 10-fold cross-validation approach with 10 repetitions. The model was initially assessed by calculating the area under the curve (AUC) score for each component of the Partial Least Squares Discriminant Analysis (PLSDA) algorithm. This was done to determine the discriminatory strength of the features. Following the evaluation of the AUC score, the association between lipidomic and proteomic features was analysed using a circle correlation plot in the DIABLO package.

Data availability

All data are available in the main text or the supplementary materials. The mass spectrometry proteomics data have been deposited to the ProteomeXchange Consortium via the PRIDE partner repository with the dataset identifier PXD049990. The lipidomic datasets are reported in supplementary data. Metabolomics datasets are available from the corresponding author upon reasonable request. Biological samples are available on reasonable request and after signed MTA.

Received: 1 March 2024; Accepted: 9 December 2024;
Published online: 24 January 2025

References

1. Bloem, B. R., Okun, M. S. & Klein, C. Parkinson's disease. *Lancet* **397**, 2284–2303 (2021).
2. Braak, H. et al. Staging of brain pathology related to sporadic Parkinson's disease. *Neurobiol. Aging* **24**, 197–211 (2003).
3. Schapira, A. H. V., Chaudhuri, K. R. & Jenner, P. Erratum: Non-motor features of Parkinson disease. *Nat. Rev. Neurosci.* **18**, 509–509 (2017).
4. Espay, A. J. et al. Biomarker-driven phenotyping in Parkinson's disease: a translational missing link in disease-modifying clinical trials. *Mov. Disord.* **32**, 319–324 (2017).
5. Galper, J. et al. Lipid pathway dysfunction is prevalent in patients with Parkinson's disease. *Brain* **145**, 3472–3487 (2022).
6. Avisar, H. et al. Lipid level alteration in human and cellular models of alpha synuclein mutations. *NPJ Parkinsons Dis.* **8**, 52 (2022).
7. Calvano, C. D. et al. Searching for potential lipid biomarkers of Parkinson's disease in parkin-mutant human skin fibroblasts by HILIC-ESI-MS/MS: preliminary findings. *Int. J. Mol. Sci.* **20**, 3341 (2019).
8. Zilocchi, M. et al. Exploring the impact of PARK2 mutations on the total and mitochondrial proteome of human skin fibroblasts. *Front. Cell Dev. Biol.* **8**, 423 (2020).
9. Shao, Y. et al. Comprehensive metabolic profiling of Parkinson's disease by liquid chromatography-mass spectrometry. *Mol. Neurodegener.* **16**, 4 (2021).
10. Gialluisi, A. et al. Whole exome sequencing study of Parkinson disease and related endophenotypes in the Italian population. *Front. Neurol.* **10**, 1362 (2020).
11. Palomba, N. P. et al. Common and rare variants in TMEM175 gene concur to the pathogenesis of Parkinson's disease in Italian patients. *Mol. Neurobiol.* **60**, 2150–2173 (2023).
12. Jinn, S. et al. Functionalization of the TMEM175 p.M393T variant as a risk factor for Parkinson disease. *Hum. Mol. Genet.* **28**, 3244–3254 (2019).
13. Jinn, S. et al. TMEM175 deficiency impairs lysosomal and mitochondrial function and increases α-synuclein aggregation. *Proc. Natl Acad. Sci. USA* **114**, 2389–2394 (2017).
14. Hu, M. et al. Parkinson's disease-risk protein TMEM175 is a proton-activated proton channel in lysosomes. *Cell* **185**, 2292–2308.e20 (2022).
15. Wie, J. et al. A growth-factor-activated lysosomal K+ channel regulates Parkinson's pathology. *Nature* **591**, 431–437 (2021).
16. Lobasso, S. et al. Lipid profiling of *parkin*-mutant human skin fibroblasts. *J. Cell Physiol.* **232**, 3540–3551 (2017).
17. Galvagnion, C. et al. Sphingolipid changes in Parkinson L444P GBA mutation fibroblasts promote α-synuclein aggregation. *Brain* **145**, 1038–1051 (2022).
18. Gruenberg, J. Life in the lumen: the multivesicular endosome. *Traffic* **21**, 76–93 (2020).
19. Ridgway, N. D. Phospholipid synthesis in mammalian cells in *Biochemistry of Lipids, Lipoproteins and Membranes*, 227–258 (Elsevier, 2021).
20. Patel, S., Homaei, A., El-Seedi, H. R. & Akhtar, N. Cathepsins: proteases that are vital for survival but can also be fatal. *Biomed. Pharmacother.* **105**, 526–532 (2018).
21. Komori, T. et al. Phosphorylation of Rab29 at Ser185 regulates its localization and role in the lysosomal stress response in concert with LRRK2. *J. Cell Sci.* **136**, jcs261003 (2023).
22. Navarro-Romero, A., Montpeyó, M. & Martinez-Vicente, M. The emerging role of the lysosome in Parkinson's disease. *Cells* **9**, 2399 (2020).
23. Fortin, D. L. et al. Lipid rafts mediate the synaptic localization of α-synuclein. *J. Neurosci.* **24**, 6715–6723 (2004).
24. Narayanan, V., Guo, Y. & Scarlata, S. Fluorescence studies suggest a role for α-synuclein in the phosphatidylinositol lipid signaling pathway. *Biochemistry* **44**, 462–470 (2005).
25. Schechter, M. et al. Synuclein facilitates endocytosis by elevating the steady-state levels of phosphatidylinositol 4,5-bisphosphate. *J. Biol. Chem.* **295**, 18076–18090 (2020).
26. Jacob, R. S., Eichmann, C., Dema, A., Mercadante, D. & Selenko, P. α-Synuclein plasma membrane localization correlates with cellular phosphatidylinositol polyphosphate levels. *Elife* **10**, e61951 (2021).
27. Singh, A. et al. DIABLO: an integrative approach for identifying key molecular drivers from multi-omics assays. *Bioinformatics* **35**, 3055–3062 (2019).
28. Cang, C., Aranda, K., Seo, Y. J., Gasnier, B. & Ren, D. TMEM175 is an organelle K+ channel regulating lysosomal function. *Cell* **162**, 1101–1112 (2015).
29. Chang, D. et al. A meta-analysis of genome-wide association studies identifies 17 new Parkinson's disease risk loci. *Nat. Genet.* **49**, 1511–1516 (2017).
30. Langmyhr, M. et al. Allele-specific expression of Parkinson's disease susceptibility genes in human brain. *Sci. Rep.* **11**, 504 (2021).
31. Grover, S. et al. Genome-wide association and meta-analysis of age at onset in Parkinson disease: evidence from the COURAGE-PD Consortium. *Neurology* **99**, E698–E710 (2022).
32. Zhao, Y. et al. Genetic analysis of six transmembrane protein family genes in Parkinson's disease in a large Chinese cohort. *Front. Aging Neurosci.* **14**, 889057 (2022).
33. Saiki, S. et al. Decreased long-chain acylcarnitines from insufficient β-oxidation as potential early diagnostic markers for Parkinson's disease. *Sci. Rep.* **7**, 7328 (2017).
34. Tarasenko, T. N., Cusmano-Ozog, K. & McGuire, P. J. Tissue acylcarnitine status in a mouse model of mitochondrial β-oxidation deficiency during metabolic decompensation due to influenza virus infection. *Mol. Genet. Metab.* **125**, 144–152 (2018).
35. Imgrund, S. et al. Adult ceramide synthase 2 (CERS2)-deficient mice exhibit myelin sheath defects, cerebellar degeneration, and hepatocarcinomas. *J. Biol. Chem.* **284**, 33549–33560 (2009).
36. van Smeden, J. et al. Intercellular skin barrier lipid composition and organization in Netherton syndrome patients. *J. Invest. Dermatol.* **134**, 1238–1245 (2014).
37. Jazvinšćak Jembrek, M., Hof, P. R. & Šimić, G. Ceramides in Alzheimer's disease: key mediators of neuronal apoptosis induced by

oxidative stress and Aβ accumulation. *Oxid. Med. Cell. Longev.* **2015**, 346783 (2015).
38. Tommasino, C., Marconi, M., Ciarlo, L., Matarrese, P. & Malorni, W. Autophagic flux and autophagosome morphogenesis require the participation of sphingolipids. *Apoptosis* **20**, 645–657 (2015).
39. Norris, G. H. & Blesso, C. N. Dietary and endogenous sphingolipid metabolism in chronic inflammation. *Nutrients* **9**, 1180 (2017).
40. Abbott, S. K. et al. Altered ceramide acyl chain length and ceramide synthase gene expression in Parkinson's disease. *Mov. Disord.* **29**, 518–526 (2014).
41. Gegg, M. E. et al. No evidence for substrate accumulation in Parkinson brains with *GBA* mutations. *Mov. Disord.* **30**, 1085–1089 (2015).
42. Pujol-Lereis, L. M. Alteration of sphingolipids in biofluids: implications for neurodegenerative diseases. *Int. J. Mol. Sci.* **20**, 3564 (2019).
43. van der Veen, J. N. et al. The critical role of phosphatidylcholine and phosphatidylethanolamine metabolism in health and disease. *Biochim. Biophys. Acta Biomembr.* **1859**, 1558–1572 (2017).
44. Listenberger, L. L. et al. Triglyceride accumulation protects against fatty acid-induced lipotoxicity. *Proc. Natl Acad. Sci. USA* **100**, 3077–3082 (2003).
45. Zhang, J., Zhang, X., Wang, L. & Yang, C. High performance liquid chromatography-mass spectrometry (LC-MS) based quantitative lipidomics study of ganglioside-NANA-3 plasma to establish its association with Parkinson's disease patients. *Med. Sci. Monit.* **23**, 5345–5353 (2017).
46. Miletić Vukajlović, J. et al. Increased plasma phosphatidylcholine/lysophosphatidylcholine ratios in patients with Parkinson's disease. *Rapid Commun. Mass Spectrom.* **34**, e8595 (2020).
47. Stoessel, D. et al. Promising metabolite profiles in the plasma and CSF of early clinical Parkinson's disease. *Front. Aging Neurosci.* **10**, 51 (2018).
48. Fanning, S. et al. Lipidomic analysis of α-synuclein neurotoxicity identifies stearoyl CoA desaturase as a target for Parkinson treatment. *Mol. Cell* **73**, 1001–1014.e8 (2019).
49. van Meer, G., Voelker, D. R. & Feigenson, G. W. Membrane lipids: where they are and how they behave. *Nat. Rev. Mol. Cell Biol.* **9**, 112–124 (2008).
50. Epand, R. M. Features of the phosphatidylinositol cycle and its role in signal transduction. *J. Membr. Biol.* **250**, 353–366 (2017).
51. Seyfried, T. N. et al. Sex-related abnormalities in substantia nigra lipids in Parkinson's disease. *ASN Neuro* **10**, 175909141878188 (2018).
52. Zhang, Z. et al. Roles of glutamate receptors in Parkinson's disease. *Int. J. Mol. Sci.* **20**, 4391 (2019).
53. Iwasaki, Y., Ikeda, K., Shiojima, T. & Kinoshita, M. Increased plasma concentrations of aspartate, glutamate and glycine in Parkinson's disease. *Neurosci. Lett.* **145**, 175–177 (1992).
54. Mally, J., Szalai, G. & Stone, T. W. Changes in the concentration of amino acids in serum and cerebrospinal fluid of patients with Parkinson's disease. *J. Neurol. Sci.* **151**, 159–162 (1997).
55. Jiménez-Jiménez, F. J. et al. Neurotransmitter amino acids in cerebrospinal fluid of patients with Parkinson's disease. *J. Neurol. Sci.* **141**, 39–44 (1996).
56. Figura, M. et al. Serum amino acid profile in patients with Parkinson's disease. *PLoS ONE* **13**, e0191670 (2018).
57. Shimmura, C. et al. Alteration of plasma glutamate and glutamine levels in children with high-functioning autism. *PLoS ONE* **6**, e25340 (2011).
58. Shinohe, A. et al. Increased serum levels of glutamate in adult patients with autism. *Prog. Neuropsychopharmacol. Biol. Psychiatry* **30**, 1472–1477 (2006).
59. Campanelli, F., Natale, G., Marino, G., Ghiglieri, V. & Calabresi, P. Striatal glutamatergic hyperactivity in Parkinson's disease. *Neurobiol. Dis.* **168**, 105697 (2022).
60. Bongarzone, E. R. et al. Insights into the pathogenesis and treatment of Krabbe disease. *Pediatr. Endocrinol. Rev.* **13**, 689–696 (2016).
61. Senkevich, K. et al. GALC variants affect galactosylceramidase enzymatic activity and risk of Parkinson's disease. *Brain* **146**, 1859–1872 (2023).
62. Nalls, M. A. et al. Identification of novel risk loci, causal insights, and heritable risk for Parkinson's disease: a meta-analysis of genome-wide association studies. *Lancet Neurol.* **18**, 1091–1102 (2019).
63. Willett, R. et al. TFEB regulates lysosomal positioning by modulating TMEM55B expression and JIP4 recruitment to lysosomes. *Nat. Commun.* **8**, 1580 (2017).
64. Hashimoto, Y., Shirane, M. & Nakayama, K. I. TMEM55B contributes to lysosomal homeostasis and amino acid–induced mTORC1 activation. *Genes Cells* **23**, 418–434 (2018).
65. Sbrissa, D. et al. Core protein machinery for mammalian phosphatidylinositol 3,5-bisphosphate synthesis and turnover that regulates the progression of endosomal transport. *J. Biol. Chem.* **282**, 23878–23891 (2007).
66. Shisheva, A. PIKfyve and its lipid products in health and in sickness in *Current Topics in Microbiology and Immunology*, 127–162 (Springer, 2012).
67. Horvath, J. D. et al. α-Synuclein-dependent increases in PIP5K1γ drive inositol signaling to promote neurotoxicity. *Cell Rep.* **42**, 113244 (2023).
68. Zhao, Y. et al. Intracellular generation of sphingosine 1-phosphate in human lung endothelial cells. *J. Biol. Chem.* **282**, 14165–14177 (2007).
69. Craft, S. et al. Intranasal insulin therapy for Alzheimer disease and amnestic mild cognitive impairment: a pilot clinical trial. *Arch. Neurol.* **69**, 29–38 (2012).
70. Talbot, K. et al. Demonstrated brain insulin resistance in Alzheimer's disease patients is associated with IGF-1 resistance, IRS-1 dysregulation, and cognitive decline. *J. Clin. Investig.* **122**, 1316–1338 (2012).
71. Ashraghi, M. R., Pagano, G., Polychronis, S., Niccolini, F. & Politis, M. Parkinson's disease, diabetes and cognitive impairment. *Recent Pat. Endocr. Metab. Immune Drug Discov.* **10**, 11–21 (2016).
72. Pang, Y. et al. Intranasal insulin protects against substantia nigra dopaminergic neuronal loss and alleviates motor deficits induced by 6-OHDA in rats. *Neuroscience* **318**, 157–165 (2016).
73. Yang, L., Wang, H., Liu, L. & Xie, A. The role of insulin/IGF-1/PI3K/Akt/GSK3β signaling in Parkinson's disease dementia. *Front. Neurosci.* **12**, 73 (2018).
74. Muschol, N. et al. Transport, enzymatic activity, and stability of mutant sulfamidase (SGSH) identified in patients with mucopolysaccharidosis type III A. *Hum. Mutat.* **23**, 559–566 (2004).
75. Nosier, S. S., El Nakeeb, S. M. S., Ibrahim, M. M., El-Gammal, M. & Fateen, E. M. Biochemical diagnosis of Sanfilippo disorder types A and B. *J. Genet. Eng. Biotechnol.* **21**, 112 (2023).
76. Akizu, N. et al. Biallelic mutations in SNX14 cause a syndromic form of cerebellar atrophy and lysosome-autophagosome dysfunction. *Nat. Genet.* **47**, 528–534 (2015).
77. Zhou, Y. et al. Altered lipid homeostasis is associated with cerebellar neurodegeneration in SNX14 deficiency. *JCI Insight* **9**, e168594 (2024).
78. Jia, J. et al. Galectin-3 coordinates a cellular system for lysosomal repair and removal. *Dev. Cell* **52**, 69–87.e8 (2020).
79. García-Revilla, J. et al. Galectin-3 shapes toxic alpha-synuclein strains in Parkinson's disease. *Acta Neuropathol.* **146**, 51–75 (2023).
80. Postuma, R. B. et al. MDS clinical diagnostic criteria for Parkinson's disease. *Mov. Disord.* **30**, 1591–1601 (2015).
81. Manfredi, M., Martinotti, S., Gosetti, F., Ranzato, E. & Marengo, E. The secretome signature of malignant mesothelioma cell lines. *J. Proteom.* **145**, 3–10 (2016).

82. Barberis, E. et al. Large-scale plasma analysis revealed new mechanisms and molecules associated with the host response to SARS-CoV-2. *Int. J. Mol. Sci.* **21**, 8623 (2020).
83. Barberis, E. et al. Understanding protection from SARS-CoV-2 using metabolomics. *Sci. Rep.* **11**, 13796 (2021).

Acknowledgements

We are grateful to the Italian Ministry of Health which supported this work by grant n. PNRR-MAD-2022-12375960 Next Generation EU - PNRR M6C2 Investimento 2.1 valorizzazione e potenziamento della ricerca biomedica del SSN to TE, by grant n. RF 2019-12370224 to TE, by Current Research to TE and partially supported by grant n. PNRR-MCNT2-2023-12377375 Next Generation EU - PNRR M6C2 Investimento 2.1 valorizzazione e potenziamento della ricerca biomedica del SSN to TE. We also thank Italian Ministry of University and Research (MUR) that partially supported the study by the project PRIN n. 2022W3RKLJ funded by European Union–Next Generation EU, by CNR project FOE-2021 DBA.AD005.225 and by CNR project INVECCHIAMENTO (DSB.AD009). This study was (partially) funded by Next Generation EU (NGEU) Italian Ministry of University and Research (M.U.R), National Recovery and Resilience Plan (NRRP), Project MNESYS (PE0000006) – A Multiscale Integrated Approach to the study of the Nervous System in Health and Disease (DN. 1553 11.10.2022). F.C. and G.F. were supported by Italian Ministry of University and Research (MUR) project PRIN n. 2022W3RKLJ funded by European Union – Next Generation EU. L.I. was supported by PNRR-MAD-2022-12375960 Next Generation EU—PNRR M6C2 Investimento 2.1 valorizzazione e potenziamento della ricerca biomedica del SSN. This study was (partially) funded by the Italian Ministry of University and Research (MUR) program "Departments of Excellence 2023-2027", AGING Project—Department of Translational Medicine, Università del Piemonte Orientale. The funders had no role in study design, data collection and analysis, decision to publish, or preparation of the manuscript.

Author contributions

T.E., F.C. and M.M. designed the study. N.M., S.P., T.G. and N.P.P. recruited the patients, performed clinical study, and collected the data. N.P.P., L.I. performed sample management and biobanking. G.F. realised human dermal fibroblasts. M.G., V.D.G., E.B. and M.M. performed lipidomic, metabolomic and proteomic analysis. S.K. and M.M. performed integration analysis. F.C., M.G., V.D.G., E.B., M.M. and T.E. performed bioinformatic and statistical analysis of omics data. F.C. and T.E. performed the correlation analyses. F.C. and T.E. wrote the manuscript. All authors revised the final manuscript.

Competing interests

The authors declare no competing interests.

Additional information

Supplementary information The online version contains supplementary material available at https://doi.org/10.1038/s41531-024-00853-5.

Correspondence and requests for materials should be addressed to Teresa Esposito.